Sofia University "St. Kliment Ohridski"
Faculty of Physics
Department of „Radiophysics and Electronics“

Abstract

for the dissertation
„Conversion of CO_2 using Arc Discharges at Atmospheric Pressure“

Vladislav Valentinov Ivanov

Specialty: „Radiophysics and physical electronics“
4.1 Physical sciences

Research supervisor:
/**Assoc. prof. Dr. Stanimir Kolev**/

Sofia, Bulgaria
January 26, 2023

Introduction

Carbon dioxide is a gas that forms when carbon compounds burn, and has played a major role in the past and present state of the Earth's atmosphere, biosphere, etc. It is most often associated with the environmental problem of the global increase in the average temperature in the lower layers of the atmosphere, through the so-called greenhouse effect. According to [1], from the middle of the 19th century until today, the concentration of carbon dioxide in the atmosphere has increased from 250 ppm to over 400 ppm, and this increase is mainly associated with society's transition to industrialization.

The conversion of carbon dioxide into various useful substances is of interest to both the industry and ecology. Through various chemical processes, methane CH_4, methanol CH_3OH, oxygen O_2 and others can be produced from CO_2.

The use of low-temperature plasma discharges for the dissociation is a popular and effective method [2]. Direct current discharges, dielectric barrier discharges (DBD) [3, 4, 5, 6], microwave (MW) discharges [7, 8, 9, 10] and others can be used. Direct current discharges can be used both for thermal conversion, through plasma torches (plasma torch, plasmatron) [11], and for low-temperature conversion. Impulse discharges, in which a large amount of power is applied for short intervals of time, are also being researched. Dielectric barrier discharges can operate at atmospheric pressure, but under such conditions they exhibit low efficiencies ($< 20\%$). Microwave discharges can reach high conversion values ($> 80\%$ [10]), but are only effective at low gas pressures.

This PhD is related to the study of direct current discharges as a means of dissociating carbon dioxide. Specifically, discharges operating at atmospheric pressure and low power (< 1000 W). The work is motivated by improving the understanding of the dissociation process through this type of discharges, as good dissociation rates can easily and efficiently be achieved with them, at atmospheric pressure. The fact that they operate efficiently at atmospheric pressure, makes the cost of their implementation and operation lower. Such technologies could be applied on an industrial scale, which would potentially have benefits from an ecological point of view.

Application of arc discharges for carbon dioxide dissociation One of the frequently studied direct current discharges in the field of dissociation is the so-called gliding arc discharge. Experimental studies of gliding arc (GA) discharges include [12, 13, 14, 15, 16, 8]. These discharges can create non-equilibrium plasma, in which the electron temperature is much higher than the gas one. Typically, the electron temperature in this type of plasma is of the order of several eV (10^4 K), and the gas temperature reaches $1000 - 2000$ K. The high electron density of $10^{18} - 10^{20}$ m^{-3} and the high electron temperature of $1 - 5$ eV allow the conversion to take place via stepwise vibrational dissociation, a mechanism that has been identified as an efficient dissociation channel at low gas temperatures in [17, 18, 19].

Additionally, gliding arc discharges can be controlled using permanent external magnetic fields. The use of magnetic fields to direct and control electric arcs in gases is an old method used as far back as the early 20th century. For example [20] – such a reactor is used for nitrates production. In more recent developments [21], this approach is used

in low current devices to control the gas flow through the discharge. There are several studies of arc discharges with magnetic manipulation for treatment of gases, including [22, 23, 24, 25, 26, 27]. Many of them are implemented in a cylindrical configuration with two concentric electrodes. The use of magnetic fields has also been investigated in a gliding arc type of discharge, with flat diverging electrodes [28].

Aims and objectives of the current dissertation The aim of the current dissertation is to investigate the properties of low-current ($30 - 200$ mA) DC discharges in the gliding arc and magnetically stabilized configurations, at atmospheric pressure. Specifically, their applicability for the dissociation of carbon dioxide is investigated, with the theoretical studies done, being qualitatively valid for a wider range of discharge configurations and conditions. Gliding arc discharges have been used in numerous studies for CO_2 conversion, such as in [12, 13, 14]. In some of them [12, 16, 8], it has been shown that low-current DC discharges can reach dissociation efficiency of $40 - 50\%$, thus achieving dissociation levels above 10% at power values below 1 kW, at atmospheric pressure.

A substantial part of the present work is devoted to research of low-current DC discharges with magnetic stabilization and magnetic acceleration (such as [28] and others), as a problem both from a fundamental point of view and in the context of their application for carbon dioxide dissociation. The discharge considered and used in the our work is implementing the classic two-dimensional configuration with diverging electrodes, since with this kind of a device, it is convenient to realize, investigate and compare configurations with magnetic fields (with magnetic stabilization and magnetic acceleration), to the classical gliding arc discharge.

The work on this dissertation includes the computer modeling of a magnetically stabilized arc discharge and experimental studies of several types of low current discharges, for the dissociation of CO_2. Experiments include gliding arc discharges (without magnetic stabilization), as well as magnetically accelerated discharges. The dissertation tasks are defined as follows:

1. Creation of a two-dimensional computer model of a section of the positive column of a magnetically stabilized arc, in the conditions of a constant electric field, at atmospheric pressure, in argon, for a laminar gas flow and a current of $50 - 400$ mA. Investigating the effect of the gas flow and the magnetic force on the behavior of the arc.

2. Realization of an experimental installation, including a high-voltage electrical power supply, a gas discharge device for testing arc discharges at atmospheric pressure, a water cooling system and other components.

3. Carrying out a large series of experimental measurements of different discharge configurations, for CO_2 dissociation at atmospheric pressure at low currents ($25 - 200$ mA).

4. Investigation of the discharge behavior and the properties of low current DC discharges (< 200 mA), in the classic gliding arc configuration and the magnetically enhanced setups.

Structure of the dissertation document The dissertation mainly consists of three chapters. Chapter 1 describes the different types of direct current discharges, as well as the modeling of plasma processes at the macroscopic level. Also, a summary is made, of some characteristics of the carbon dioxide molecule and the specifics of its dissociation. Some implementations of plasma discharges for CO_2 dissociation are briefly summarized. In chapter 2 of the dissertation, a numerical fluid model of the cross section of the positive column of a magnetically stabilized arc discharge is presented. Chapter 3 includes experimental work for the doctorate, on the study of the dissociation of CO_2. An additional section is included in this chapter, describing another type of plasma setup, not directly related to the current experimental results, through which the work on this PhD can potentially be continued in the future. In the last part of the dissertation, the contributions for the doctoral studies are presented, as well as a list of publications and participation in events.

General information about the CO_2 molecule

The CO_2 molecule is linear, consisting of two oxygen atoms and one carbon atom. The carbon atom has 6 electrons in orbitals $(1s)^2(2s)^2(2p)^2$, and the oxygen atom has 8 electrons occupying orbitals $(1s)^2(2s)^2(2p)^4$. In total, the carbon dioxide molecule has 16 valence electrons, and $3 \times 4 = 12$ molecular orbitals, of which the following are occupied: $(1\sigma_g)^2, (1\sigma_u)^2, (2\sigma_g)^2, (2\sigma_u)^2, (1\pi_u)^4(1\pi_g)^4$.

A quantum mechanical description of the carbon dioxide molecule involves consideration of the various discrete levels of the molecule's electronic states, as well as vibrational and rotational excited levels. The ground electronic state of the CO_2 molecule is marked as $^1\Sigma^+$, with the letter Σ corresponding to a zero projection ($L_z = 0$) of the total electron orbital angular momentum $L = \sum l_i$, on the axis connecting the atoms – $\Lambda\hbar = L_z = 0$, where l_i is the orbital angular momentum for the individual electrons, and Λ is a quantum number describing the discrete level of the molecular electron angular momentum. Each electronic level has associated discrete levels of vibrational motion, which may be symmetric, asymmetric or bending modes. The total energy of the molecule E is determined by these states. It can be expressed as the sum $E = E_{\text{el}} + E_{\text{vib}} + E_{\text{rot}}$, with the following dependence: $E_{\text{el}} > E_{\text{vib}} > E_{\text{rot}}$, between the energies of the electronic state, and the vibrational and rotational modes. The vibrational excited state can be written as $CO_2(\nu_1, \nu_2^{l_2}, \nu_3)$, in terms of three quantum numbers for the energy level.

Dissociation of CO_2

The dissociation reaction has the form $CO_2 \rightarrow CO + \frac{1}{2}O_2$, and in most sources it is assumed that the enthalpy of the reaction is $\Delta H = 2.9$ eV/mol. This reaction can be carried out mainly in two ways. By increasing the temperature of the gas (up to thousands of kelvins) - the so-called thermal dissociation or by non-thermal processes involving electrons.

Thermal conversion requires heating the gas to high temperatures, on the order of 10^3 K, which can be quite inefficient. At low temperatures (below 600 K), the reaction reaches its equilibrium and under these conditions, its contribution to the total dissociation is negligible. Thermal conversion can be accomplished by plasma torches and high-pressure radio frequency discharges. In the thermal conversion, all degrees of freedom of the molecule (vibrational, rotational) receive an equal part of the thermal energy, but only some of them contribute to the dissociation. From this follows, that there is an upper bound for the energy efficiency of about 40% (Levitsky and Butylkin et al., 1978, 1979 [29]).

Non-thermal processes include direct electron-impact dissociation and electron-attachment dissociation. Dissociation by non-thermal plasma has its advantages, mainly related to the efficiency of the process [2, 29]. Direct dissociation by electron impact is a one-step process, from which a carbon monoxide molecule is obtained as a product, in a non-ground electronic state. This dissociation mechanism is essential at low pressure, requiring the participating electron to have an energy of about 14 eV. Electron attachment dissociation has a small contribution to the total dissociation, but it helps to maintain the charge balance in the plasma.

The dissociation of the CO_2 molecule can be performed by stepwise excitation of the vibrational states, of the ground electronic state of the CO_2 molecule. This mechanism is the most efficient dissociation channel in low-temperature plasma. This stems from the fact that even electrons with a relatively low energy ($\approx$ 1 eV), several times lower than the direct dissociation energy ($11 - 14$ eV/molecule), manage to transfer almost all of their energy to the vibrational degrees of freedom of the molecule. In this way, most of the energy introduced into the discharge is selectively transferred to a specific dissociation channel – through the vibrational states of the molecule. Since the reaction rate of electronic excitation of the molecule is higher than that of vibrational-translational (VT) relaxation, it follows that there is a positive increase in the energy of the vibrational states as a result of electron collisions.

Electrons from the plasma, through vibrational excitation, mostly increase the population of the lower vibrational levels of the ground electronic state. The population of the higher excited vibrational levels is due to the vibrational-vibrational (VV) interaction processes. When CO_2 molecules with a high levels of vibrational excitation gain energy above the dissociation threshold, they can dissociate. In stepwise vibrational dissociation, the dissociation energy required exactly corresponds to the C=O bond energy (5.5 eV). The oxygen atom created in this dissociation can then engage in a second reaction, with another vibrationally excited CO_2 molecule, to produce a second CO molecule and molecular oxygen. This reaction is faster than the three-particle recombination ($O + O + M \rightarrow O_2 + M$) and allows a second CO molecule to be produced for one dissociation event. The main contribution to the dissociation by excitation of vibrational levels is from the upper asymmetric vibrational levels.

Experimental studies of the dissociation of CO_2 by means of plasma discharges

In the late 1970s and early 1980s, numerous studies of various types of plasma discharges in carbon dioxide were conducted in the Soviet Union. These developments are summarized in [29]. Studies, for both thermal and non-thermal dissociation, have been carried out for various pressures in the range up to 300 Torr. Glow discharges, microwave and radio frequency discharges have been tested.

From the point of view of the industrialization of such systems, discharges that can operate at atmospheric pressure are preferable. Dielectric barrier discharges (DBDs), studied in [3, 4, 5, 6] and others, can operate under atmospheric conditions, but at low efficiencies <20%, as it is claimed that at they cannot achieve the stepwise vibrational dissociation [2]. There is great interest in gliding arc discharges (GA). Some of the studies of gliding arc discharges include [12, 13, 14, 15, 16, 30]. Figure 1 compares the different types of discharges for their qualities as means for carbon dioxide dissociation. This comparison is based on many different sources and is described in more detail in [2]. It shows that GA discharges at atmospheric pressure achieve good results, comparable to microwave discharges at low pressures.

In the context of carbon dioxide dissociation, gliding arc discharges have been investigated in [12, 13, 14, 31] and others. Another variety of gliding arc discharges are the gliding discharges in the so-called three-dimensional configuration, which are usually realized with a pair of concentric electrodes. Most of these devices are a cylindrical tube,

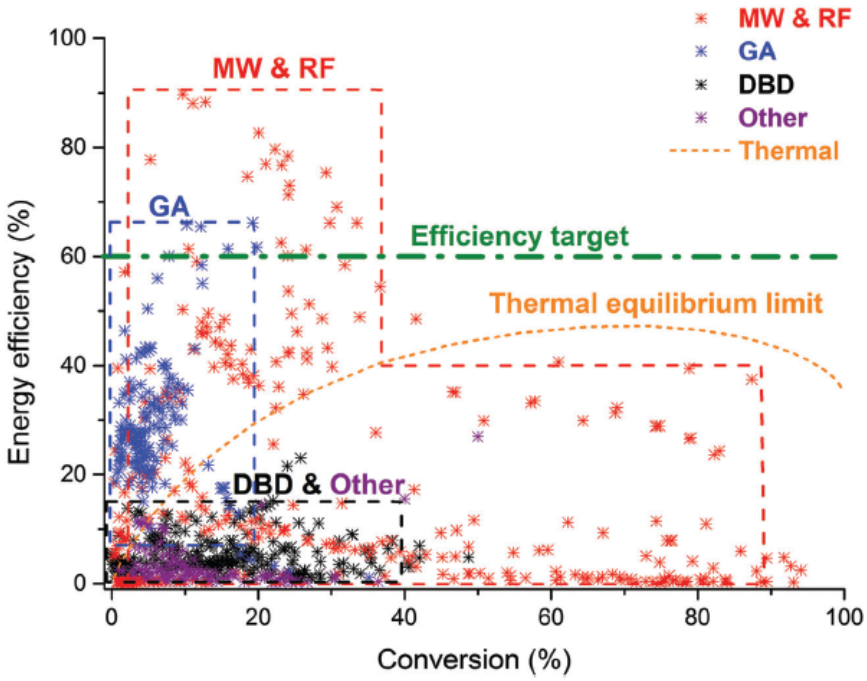

Figure 1: Comparison using two of most commonly measured dissociation quantities – percent of converted gas (abscissa) and energy efficiency (ordinate). Comparison between different types of discharges, based on numerous literature sources. The orange dashed line shows the theoretical limit for thermal conversion.

in which the gas flow is usually fed axially or tangentially. Developments of such three-dimensional configurations are for example [16, 30, 32], as well as variations using an axial external magnetic field [15].

Modeling of an arc discharge with magnetic stabilization in argon

The content of chapter 2 of the dissertation is shown here in abbreviated form. It presents a numerical model with which a configuration of a low-current arc (under 1 A), operating at direct current, in argon gas flow at atmospheric pressure, was investigated. This study was published in [B.1]. The motion of the arc (positive column) is constrained by a time-constant magnetic field, perpendicular to both the external electric field and the directional gas velocity. The movement of the arc is further limited by two side walls, that prevent it from moving or extending too much in a direction perpendicular to the gas flow. Although the investigated gas is argon and not CO_2, the results presented in chapter 2 of the dissertation, can be used for the understanding of low-current DC magnetically stabilized arcs in more general terms.

For a given interval of gas velocities and for a constant value of the magnetic flux density, the arc stabilizes and becomes localized, with quasi-stationary parameters in time. Its position remains constant and is determined by the balance of the effective drag force of the arc with the gas and the magnetic force that the arc experiences from the

external magnetic field. Because of the chosen orientation of the external magnetic field, relative to the current, these two forces act in opposite directions. For the case where the arc succeeds in stabilizing itself in the described manner, we say that it is „magnetically stabilized“. The stabilization method with an external magnetic field, allows for the ability to control the arc velocity relative to the gas, but more importantly it provides a way to maintain a constant (in time), localized (in space) plasma channel, of near-constant power and therefore of constant ionization.

The simulation model is based on a real laboratory device, which is also the subject of the research of the current dissertation and is presented in chapter 3 of the dissertation. This device is based on a gliding arc discharge [29], with additional permanent magnets providing a magnetic field between the electrodes perpendicular to the electric field. Even before the real laboratory device was tested, the results of the performed simulations showed that for the gas velocity intervals of interest to us (< 20 m/s), for currents of $\sim 10^{-1}$ A, a magnetically stabilized arc can be maintained and that the configuration studied can be used for gas processing, as the model-predicted arc temperatures exceeded those required for thermal dissociation. The analysis of the simulation data helped to answer many questions related to the stability of the arc, the distribution of the power density in the arc and the macroscopic properties of the system as a whole. The results show a significant influence of the walls on the stabilization of the arc. The case without walls (or walls located at a sufficiently large distance from the arc) was also studied, i.e. infinitely wide channel. In this case the arc becomes a source of instabilities in the gas and the appearance of vortices is observed.

The equations of the numerical model are solved using the finite element method, on a triangular grid and the time integration is performed by an implicit Euler scheme (BDF). For each time step, several iterations are performed on the solution of the system of equations, until the error in the solution falls below some threshold. The program is implemented with the Comsol Multiphysics® package (version 5.3).

Model description

Spatial configuration

The domain $\mathbf{\Omega}$ is defined as a rectangle in the $\mathbf{XY}$ plane, with width $\mathbf{W}_\mathrm{D}$ and height $\mathbf{H}_\mathrm{D}$. The motion of the arc is limited to the domain region $\mathbf{\Omega}$. The four domain boundaries are labeled as $\mathbf{W}_\mathrm{T}$, $\mathbf{W}_\mathrm{R}$, $\mathbf{W}_\mathrm{B}$ and $\mathbf{W}_\mathrm{L}$, as seen in Figure 2a. The model simulates a cross-section of the positive column of an arc discharge (or glow discharge), neglecting the effects near the electrodes. The distance between the electrodes is assumed to be $d_z = 20$ mm. The side walls of the domain are considered dielectric, at room temperature. In the domain $\mathbf{\Omega}$, there is a laminar gas flow, with the gas velocity perpendicular to the arc current and parallel to the boundary of the electrodes and the side dielectric walls. A permanent external magnetic field is applied, which is perpendicular to the arc current and the gas flow.

In the current model, the inflow has a parabolic profile in the $\mathbf{x}$-direction (shown in Figure 2b), with a maximum in the middle of the domain ($\mathbf{x} = 0$).

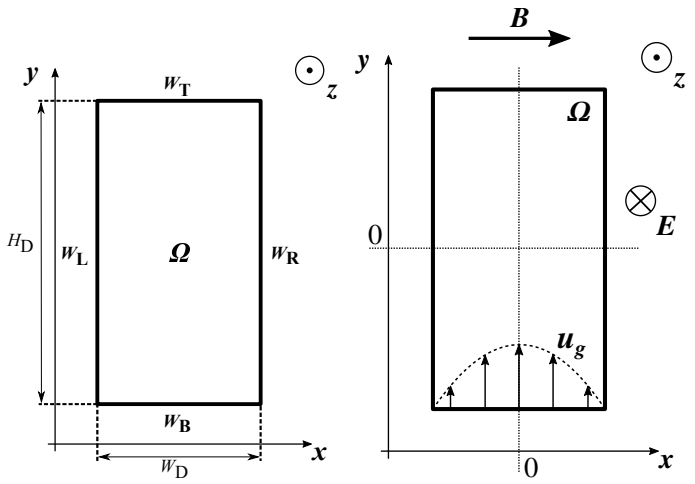

(a) (b)

Figure 2: Spatial configuration diagram of the model: (a) boundaries and dimensions; (b) magnetic field vector $\mathbf{B}$, electric field vector $\mathbf{E}$, gas velocity profile $\mathbf{u}_\mathrm{g}$ at the lower boundary $\mathbf{W_B}$.

The external electric field $\mathbf{E}$ and magnetic field $\mathbf{B}(x, y)$ are perpendicular to each other at every point (x, y) in $\mathbf{\Omega}$ and have the following components: $\mathbf{E} = [0, 0, E_z(x, t)], \mathbf{B} = [B_x(y), 0, 0]$. The transverse **z**-component of the electric field has a Gaussian profile in the **x**-direction obtained from an electrostatic simulation of the three-dimensional configuration of the electrodes. The magnetic flux density component B_x is assumed to be constant in time and is constrained similarly to $\mathbf{E}$ – by introducing a spatial distribution in the form:

$$B_x(y) = 0.6\ (\mathrm{T}) \exp\left[-\frac{1}{2}\frac{y^2}{(8\ (\mathrm{mm}))^2}\right]. \tag{1}$$

Equations for the plasma system

The types of plasma particles considered in this model are the following: argon atoms Ar, argon ions Ar^+ (ionization energy 15.76 eV), argon molecular ions Ar_2^+ (ionization energy 14.5 eV) and excited atoms for the $Ar(4s)$ atomic level (excitation energy 11.65 eV), which combines all $4s$ levels as one lumped excitation level.

The density n_s for particle type s, are calculated using the particle balance equation:

$$\frac{\partial n_s}{\partial t} + \nabla.\mathbf{\Gamma_s} + \nabla.(n_s \mathbf{u}_\mathrm{g}) = R_s. \tag{2}$$

Here $\mathbf{\Gamma_s} = n_s \mathbf{u_s}$ is the flux density for the particles (relative to the gas velocity), and is defined by the drift-diffusion approximation. The right-hand term R_s is the combined source term for the species s.

In chapter 2 of the dissertation, expressions for the mobility $\hat{\mu}_\mathbf{s}$ and diffusion $\hat{\mathbf{D}}_\mathbf{s}$ quantities are given for each type of particle. In the model a total of 14 reactions between the

particles are considered. The values for the rate coefficients, for the interactions between the electrons and the heavy particles, were calculated using the program BOLSIG+, which approximates a local solution for the Boltzmann equation. The reactions and their rate coefficients are presented in tables 2.1 and 2.2 of the dissertation document.

Using equation 2, the densities for almost all types of particles are calculated, namely: electrons, Ar^+ ions and excited $Ar(4s)$ atoms.

Equation for the density of neutrals The neutral gas density n_{Ar} is calculated directly from the equation of the ideal gas state as: $n_{Ar} = p_0/k_{\mathrm{B}}T_{\mathrm{g}}$, where T_{g} is the gas temperature, p_0 is the gas pressure (remaining constant = 1 atm) and k_{B} is the Boltzmann constant.

Quasi-neutrality condition In our implementation of the model, the minimum linear size of the discrete elements is chosen to be on the order of tens of micrometers. This size remains orders of magnitude larger than the Debye radius, under the conditions considered in the model ($\sim 10^{-8}$ m). This consideration allows us to add an additional constraint to our model, by introducing the electroneutrality condition: $n_e = n_{Ar^+} + n_{Ar_2^+}$ Thus, equation 2 is solved only for n_e, n_{Ar^+}, $n_{Ar(4s)}$, and $n_{Ar_2^+}$ is obtained from the electroneutrality condition.

Electron energy balance equation For our model the electron energy balance equation is also included, in the form:

$$\begin{aligned} &\frac{\partial n_e\langle\varepsilon_e\rangle}{\partial t} + \nabla.(\hat{\mu}_{\varepsilon,\mathbf{e}} n_e\langle\varepsilon_e\rangle\mathbf{E} - \hat{\mathbf{D}}_{\varepsilon,\mathbf{e}}\nabla n_e\langle\varepsilon_e\rangle) + \nabla.(\mathbf{u}_{\mathrm{g}} n_e\langle\varepsilon_e\rangle) = \\ &= -n_e\mathbf{u}_{\mathbf{e}}.\mathbf{E} + n_e\langle\Delta\varepsilon_e\rangle + Q_{\mathrm{bg}}, \end{aligned} \tag{3}$$

where $\langle\Delta\varepsilon_e\rangle$ expresses the electron energy losses in the various reactions, $\hat{\mathbf{D}}_{\varepsilon,\mathbf{e}}$ is the electron energy diffusion tensor and $\hat{\mu}_{\varepsilon,\mathbf{e}}$ is the electron energy mobility tensor. Expressions for these quantities are presented in the dissertation document.

For this model, an artificial background plasma is maintained through the Q_{bg} term (in equation 3), together with additional source terms in the particle balance equations (equation 2). The inclusion of this artificial background plasma reduces the gradients of the variables at the arc boundary, and thus the discretization grid can be choisen to be less dense, reducing computational times.

Current conservation equation

As an addition to the quasi-neutrality constraint $\rho(\mathbf{r}) = 0, \mathbf{r} \in \Omega$, an equation for the conservation of the current is added to the system of equations:

$$\nabla.\left[-\sigma_{\mathrm{p}}(\nabla V) + \mathbf{j}_{\mathrm{diff}} + \mathbf{j}_{\mathrm{E\times B}}\right] = -\frac{\partial\rho}{\partial t} = 0, \tag{4}$$

where $\sigma_{\mathrm{p}} = e[(\mu_{Ar^+} \times n_{Ar^+}) + (\mu_{Ar_2^+} \times n_{Ar_2^+}) + (\mu_e \times n_e)]$ is the plasma conductivity, and the separate components for the current density, from the diffusion, and $((\mathbf{E}\times\mathbf{B})$ drift,

are expressed as:

$$\begin{aligned}\mathbf{j}_{\text{diff}} &= e(-D_{Ar^+}\nabla n_{Ar^+} - D_{Ar_2^+}\nabla n_{Ar_2^+} + D_e\nabla n_e),\\ \mathbf{j}_{\text{E}\times\text{B}} &= e(\mu^2_{Ar^+} + \mu^2_{Ar_2^+} - \mu^2_e)n_s B_x E_z,\end{aligned} \tag{5}$$

where it should be clarified, that the only non-zero ($\mathbf{E}\times\mathbf{B}$) component for our configuration is the y-component equal to $B_x E_z$.

Equations for the gas velocity and gas pressure

For the description of the gas dynamics, it is assumed that the gas flow coming from of the inlet nozzle is laminar, therefore the boundary condition of $\mathbf{W}_{\text{B}}$ corresponds to the configuration of a steady laminar flow in a pipe, to which a parabolic velocity profile corresponds. Inside the domain, however, the gas flow is strongly affected by the plasma discharge, and therefore it is required to solve a system of Navier-Stokes equations for compressible laminar flow:

$$\nabla.(\rho_{\text{g}}\mathbf{u}_{\text{g}}) = 0, \tag{6a}$$

$$\rho_{\text{g}}\frac{\partial \mathbf{u}_{\text{g}}}{\partial t} + \rho_{\text{g}}(\mathbf{u}_{\text{g}}.\nabla)\mathbf{u}_{\text{g}} = \nabla.\left[-p\hat{\mathbf{I}} + \eta(\nabla\mathbf{u}_{\text{g}} + (\nabla\mathbf{u}_{\text{g}})^T) - \frac{2}{3}\eta(\nabla.\mathbf{u}_{\text{g}})\hat{\mathbf{I}}\right] + \mathbf{F}. \tag{6b}$$

The quantity ρ_{g} is the density of the gas, p is the scalar pressure of the gas, η is the dynamic viscosity of the gas, $\hat{\mathbf{I}}$ is the unit tensor, and the exchange of momentum between the charged particles and the neutral gas is introduced through the volumetric force $\mathbf{F}$ (from equation 6b):

$$\begin{aligned}\mathbf{F} &= m_{e,g}\tilde{\nu}_{e,g}(\mathbf{u_e} - \mathbf{u}_{\text{g}}) + m_{(Ar^+),g}\tilde{\nu}_{(Ar^+),g}(\mathbf{u}_{(Ar^+)} - \mathbf{u}_{\text{g}}) +\\ &+ m_{(Ar_2^+),g}\tilde{\nu}_{(Ar_2^+),g}(\mathbf{u}_{(Ar_2^+)} - \mathbf{u}_{\text{g}}),\end{aligned} \tag{7}$$

where $m_{s,g}$ and $\tilde{\nu}_{s,g}$ are the reduced mass and the macroscopic momentum exchange frequency for the type of particles s and the neutral gas. The system also includes a third equation for the gas temperature T_g, having the form:

$$\rho_{\text{g}}C_{\text{p}}\frac{\partial T_{\text{g}}}{\partial t} + \nabla.(-k_{\text{g}}\nabla T_{\text{g}}) + \rho_{\text{g}}C_{\text{p}}(\mathbf{u}_{\text{g}}.\nabla T_{\text{g}}) = Q_{\text{g}}, \tag{8}$$

where C_{p} is the heat capacity of the gas, k_{g} is the gas thermal conductivity, and Q_{g} expresses the heat from elastic collisions between electrons and neutrals.

Model of the external electric circuit

One of the main parameters for the model is the total current I through the discharge. In order to be able to control the current (in the simulation), a current source is simulated, by a simple model for the external circuit, adding the following ODE to the system of equations:

$$V_c = V_{\text{src}} - R_{\text{B}}\left[\frac{V_c}{d_z}\int_{(\Omega)} S_{\text{E}}(\mathbf{r})\sigma_{\text{p}}(\mathbf{r})\text{d}\mathbf{r} + C_{\text{B}}\frac{dV_c(t)}{dt}\right], \tag{9}$$

where σ_{p} is the plasma conductivity, $S_{\text{E}}(\mathbf{r})$ is a function that defines the spatial profile of E_z electric field component, and V_{src} is the DC voltage of a simulated external voltage source.

Boundary conditions

Table 1 presents the boundary conditions for each of the model equations. The vector $\hat{\mathbf{n}}$ denotes the normal vector for the particular boundary surface. The horizontal boundaries of the domain – $\mathbf{W}_{\mathrm{L}}$ and $\mathbf{W}_{\mathrm{R}}$ are idealized walls, with zero fluxes imposed for all particle types. The temperature of these side walls remains constant, equal to room temperature. The boundary conditions on the lower and upper walls – $\mathbf{W}_{\mathrm{B}}$ and $\mathbf{W}_{\mathrm{T}}$, are set in a way that effectively makes the computational domain, as part of an infinitely long region, with a steady laminar flow. The condition on the lower boundary represents the inlet of the gas flow, and the upper boundary the outlet, where a condition of no reverse flow is imposed.

boundary	variables				
	V,$\mathbf{J}$	n_e, n_{Ar^+}, $n_{Ar(4s)}$	$n_e\langle\varepsilon_e\rangle$	$\mathbf{u_g}, u_g = \lvert\mathbf{u_g}\rvert$	T_g
W_L, W_R	$-\hat{\mathbf{n}}.\mathbf{J} = 0$	$-\hat{\mathbf{n}}.\left[\mathbf{\Gamma_s} + \mathbf{u_g} n_s\right] = 0$	$-\hat{\mathbf{n}}.\left[\mathbf{\Gamma_{\varepsilon,e}} + \mathbf{u_g} n_e\langle\varepsilon_e\rangle\right] = 0$	$u_g = 0$	$T_g = 293\mathrm{K}$
W_T	$-\hat{\mathbf{n}}.\mathbf{J}$ $= -\hat{\mathbf{n}}.\mathbf{J}_{\mathrm{E\times B}}$	$-\hat{\mathbf{n}}.\mathbf{\Gamma_s}$ $= -[\hat{\mathbf{n}}]_y\left[n_s\mu_{0,s}^2 E_z B_x\right]$	$-\hat{\mathbf{n}}.\mathbf{\Gamma_{\varepsilon,e}}$ $= -[\hat{\mathbf{n}}]_y\left[n_e\langle\varepsilon_e\rangle\mu_{\varepsilon_e,0}\mu_{e,0}E_z B_x\right]$	$\hat{\mathbf{n}}A = -p_0\hat{\mathbf{n}}$, $A = \left[-p\hat{\mathbf{I}} + \eta\left(\nabla\mathbf{u_g} + (\nabla\mathbf{u_g})^T\right) - \frac{2}{3}\eta(\nabla.\mathbf{u_g})\hat{\mathbf{I}}\right]$	$-\hat{\mathbf{n}}.(k_g\nabla T_g) = 0$
W_B	$V = 0$			$\mathbf{u_g} = -u_{\mathrm{g,max}}\left[1 - \left(\frac{x}{W_D/2}\right)^2\right]\hat{\mathbf{n}}$	$T_g = 293\mathrm{K}$

Table 1: Boundary conditions for the model equations. The computational domain boundaries are shown more clearly on figure 2a.

Results from numerical simulations

Using the realized numerical model, non-stationary solutions were found for several different simulation configurations. Each simulation has a unique set of three input parameters. These are: *the domain width* $\mathbf{W}_{\mathrm{D}}$*, the resistance* R_{B} *(which limits the maximum current* I*, in the circuit) and the maximum gas velocity on the boundary* $\mathbf{W}_{\mathrm{B}}$ – $\mathbf{u}_{y,\mathrm{inlet}}$, for the gas inlet flow.

Table 2: Values for the input parameters for the simulations. The last column shows the intervals for which magnetic stabilization is achieved for the arc.

$\mathbf{W}_{\mathrm{D}}$ [mm]	R_{B} [kΩ]	I [mA]	$\mathbf{u}_{y,\mathrm{inlet}}$ (interval for stabilization) [m/s]
2	50, 25, 12.5	$\approx 100, 200, 400$	$1 - 2.4$
4	50, 25, 12.5	$\approx 100, 200, 400$	$1 - 7$
20	50, 25, 12.5	$\approx 100, 200, 400$	$1 - 4$

The list of calculated quantities in the simulations, of interest for the analysis, includes:

- $n_{\mathrm{e,max}} = \max_{\mathbf{\Omega}}(n_e)$ [m^{-3}]: The maximum electron density in the domain $\mathbf{\Omega}$.
- $\langle T_{\mathrm{g}}\rangle$ [K]: The average temperature of the neutral gas in the region $\mathbf{\Omega}$.

- r_{arc} [m]: Effective arc radius. It is determined from the equation:

$$\max_{\mathbf{\Omega}}(n_e)\pi r_{\text{arc}}^2 = \int_{\mathbf{\Omega}'} n_e \mathrm{d}\mathbf{\Omega}' \tag{10}$$

  or as the radius of a cylinder with height $\max_{\mathbf{\Omega}}(n_e)$, with a volume that can enclose the net electron charge in the subregion $\mathbf{\Omega}'$ (the region of the arc).

- $F_{\text{D,arc}}$ [N/m]: Drag force of the arc with the neutral gas, per unit length:

$$F_{\text{D,arc}} = -\int_{\mathbf{\Omega}'} \mathbf{F} \mathrm{d}\mathbf{\Omega}', \tag{11}$$

- $\mathbf{x}_{\text{arc}}$ and $\mathbf{y}_{\text{arc}}$: arc position. It is defined as the position of the point of maximum electron density ($\max_{\mathbf{\Omega}}(n_e)$).

The region $\mathbf{\Omega}'$ is the part of the computational domain Ω, where the electron density n_e is above 10^{17} m^{-3}.

Study of the arc behavior at different spacings between the side walls of the domain

The first part of the results shows a qualitative picture of the discharge behavior, for the different values of the domain width $\mathbf{W}_{\text{D}}$ (distance between the side walls). This parameter was found to affect the arc behavior most significantly. Its value determines the size of the arc, its position, and others.

Small distance between walls Figures 3 and 4 show the distribution of the main quantities, for the cases of $\mathbf{W}_{\text{D}} = 2$ mm and $\mathbf{W}_{\text{D}} = 4$ mm, for identical current values of $I = 200$ mA.

For the wall distance of $\mathbf{W}_{\text{D}} = 2$ mm, the arc is localized in the center of the domain, with two symmetric gas flow channels on either side. The radius of the arc is comparable to the distance between the side walls. The cooling of the gas by the walls determines the spatial profile of the gas temperature and significantly affects the position of the arc. In the literature this is usually referred to as a wall-stabilized arc.

In the case of a side wall spacing of 4 mm, the arc deviates to one of the side walls. Initially, the arc is created in the middle of the domain, but due to the parabolic profile of the gas velocity (with a maximum again in the middle $x = 0$ mm), this initial state is unstable and the arc moves to one of the vertical walls to the side. This displacement can be caused by an instability of any kind. In the physical world, such an effect can be caused by any small turbulence or asymmetry in the gas flow, while in the numerical model it is most often the result of small numerical errors or asymmetries in the grid.

Large distance between the walls In additional tests, with large side wall distances of $\mathbf{W}_{\text{D}} = 20$ mm, the goal is to exclude the effect of the walls on the arc behavior entirely. A slip boundary condition is imposed on the side walls and the heat flow to them is set to zero. The solution domain effectively has infinite width, with the velocity in the **x**-direction being constant.

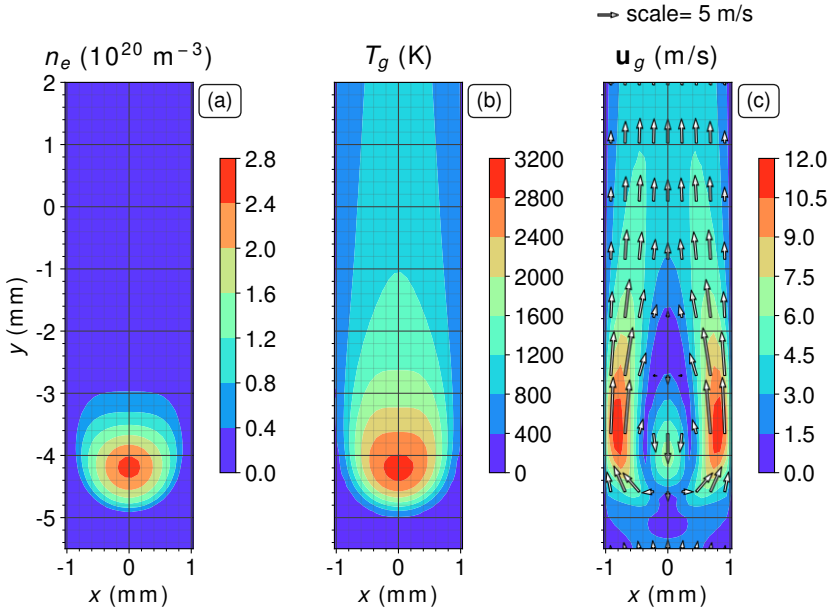

Figure 3: Spatial distribution, $\mathbf{W}_\mathrm{D} = 2$ mm, $I = 200$ mA, $\mathbf{u}_{y,\mathrm{inlet}} = 2$ m/s: (a) n_e; (b) T_g; (c) gas velocity magnitude (color) and vector field (arrows). The scale of the gas velocity vectors is given above the figure.

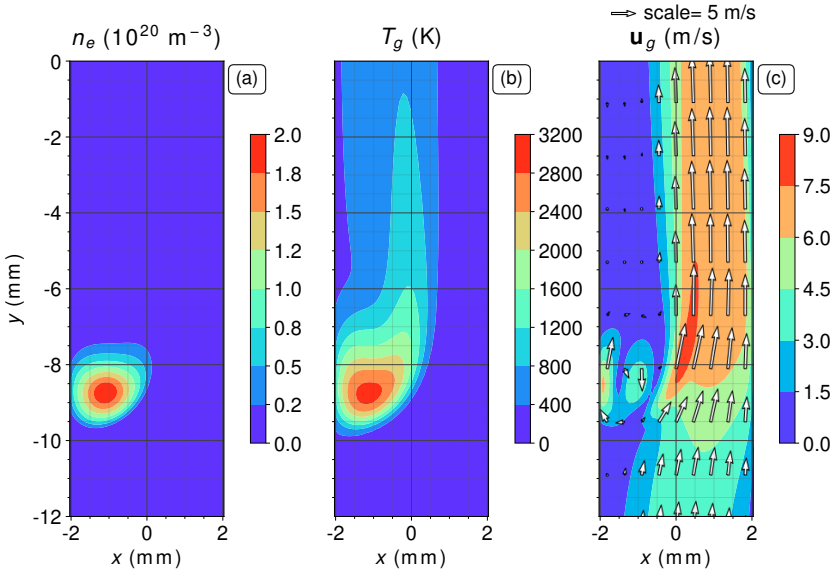

Figure 4: Spatial distribution, $\mathbf{W}_\mathrm{D} = 4$ mm, $I = 200$ mA, $\mathbf{u}_{y,\mathrm{inlet}} = 4$ m/s: (a) n_e; (b) T_g; (c) gas velocity magnitude (color) and vector field (arrows). The scale of the gas velocity vectors is given above the figure.

Test results for 20 mm widths show a behavior that is very different from the one observed in the cases for small channel widths (2 mm and 4 mm). The arc remains localized in the center of the domain, with periodic oscillation in the **x**-direction.

A vortex street is formed in the wake of the arc. The movement of the arc and the

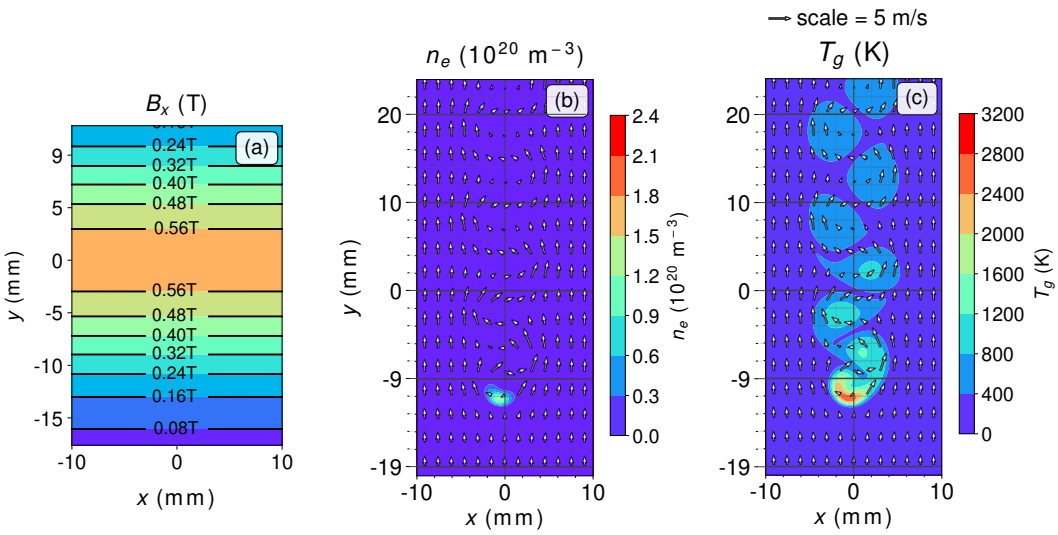

Figure 5: Spatial distribution, $\mathbf{W}_\mathrm{D} = 20$ mm, $I = 200$ mA, $\mathbf{u}_{y,\mathrm{inlet}} = 2$ m/s. Subfigure (a) shows the spatial distribution of the magnetic flux density, (b) n_e; (c) T_g. The arrows indicate the gas velocity field, with the scale of the arrows given above the figure.

dynamics of the generated vortices are closely related. The arc does not have well-defined boundaries, shape or position, and the gas in its volume is subjected to additional volume forces. The formation of vortices causes the arc to move towards the lower pressure regions, resulting in the observed oscillations („flutter instability“ [33]).

Dependence of the measured quantities to the gas flow velocity

Depending on the gas velocity (for distances between the side walls of 20 mm), from figure 6(a), it can be seen that under identical conditions, the increase in the gas flow rate leads to an increase in the frequency of transverse oscillations in the **x**-direction. The increase in frequency follows the Strouhal relation (formula 3.2 of [33]). In figure 6(b), it is shown that as the current increases and accordingly the magnetic force experienced by the arc, the frequency of these oscillations tends to decrease.

From figure 7(a), it can be seen that the average gas temperature $\langle T_\mathrm{g} \rangle$ (averaged over the entire domain), decreases with the increase in the inlet gas velocity. It can also be observed that $\langle T_\mathrm{g} \rangle$ increases with current, which is an effect of the larger power input to the discharge. The maximum electron density $n_{e,\mathrm{max}}$ tends to increase slightly with the gas velocity, as seen on figure 7(b). From figure 7(c), it is visible that the effective arc radius r_arc decreases with the gas velocity, but grows with the current. The maximum electron density and maximum current density remain almost constant, so it follows that for a larger current the arc will have a larger area and a larger radius.

From our results, an estimate was made of the effective drag coefficient C_D. Its values (shown in figure 7(d)) vary over a large interval. Compared to other sources [33], the closest matching values are obtained at $\mathbf{W}_\mathrm{D} = 2$ mm. It was also established that C_D decreases with the gas velocity. It should be noted that the presented here values for the coefficient C_D, are only a rough estimate.

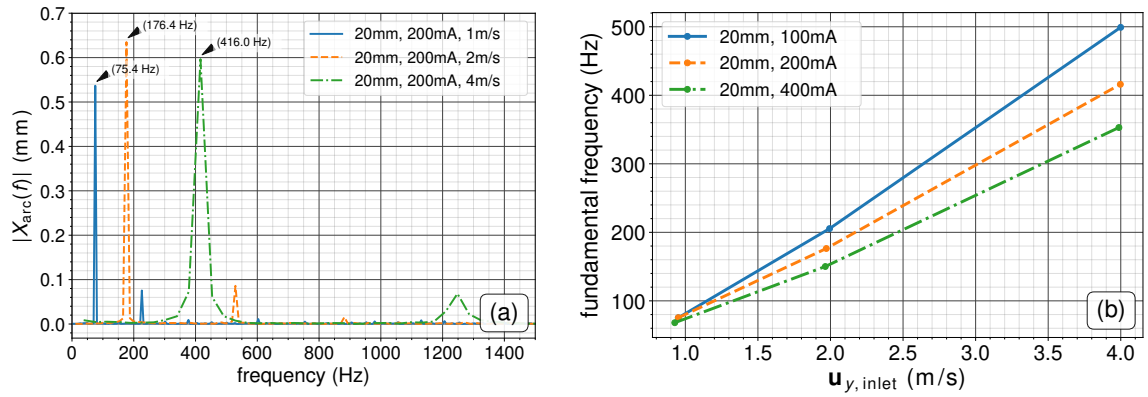

Figure 6: Amplitude spectrum of the arc oscillation in the $\mathbf{x}$-direction (a), for the case of $\mathbf{W}_{\mathrm{D}} = 20$ mm, $I = 200$ mA. Fundamental frequencies of arc oscillation in $\mathbf{x}$-direction, as a function of gas flow rate (b), for all 20 mm configurations.

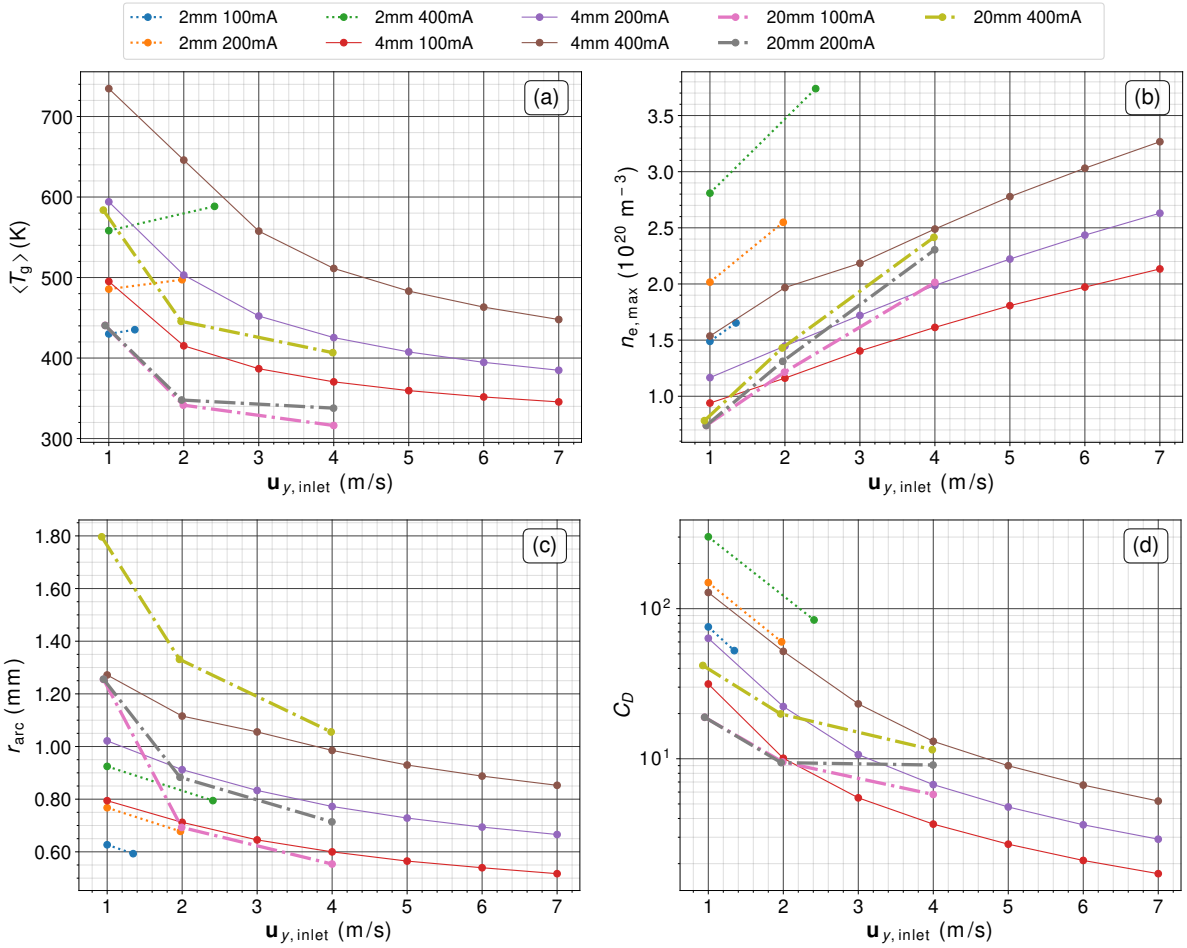

Figure 7: Average gas temperature $\langle T_{\mathrm{g}} \rangle$ (a), maximum electron density $n_{e,\mathrm{max}}$ (b), effective arc radius r_{arc} (c) and effective drag coefficient C_{D}(d), as a function of the inlet gas velocity $\mathbf{u}_{y,\mathrm{inlet}}$.

Figure 8(a) shows the $\mathbf{y}$-position of the arc, in the cases when stabilization is achieved.

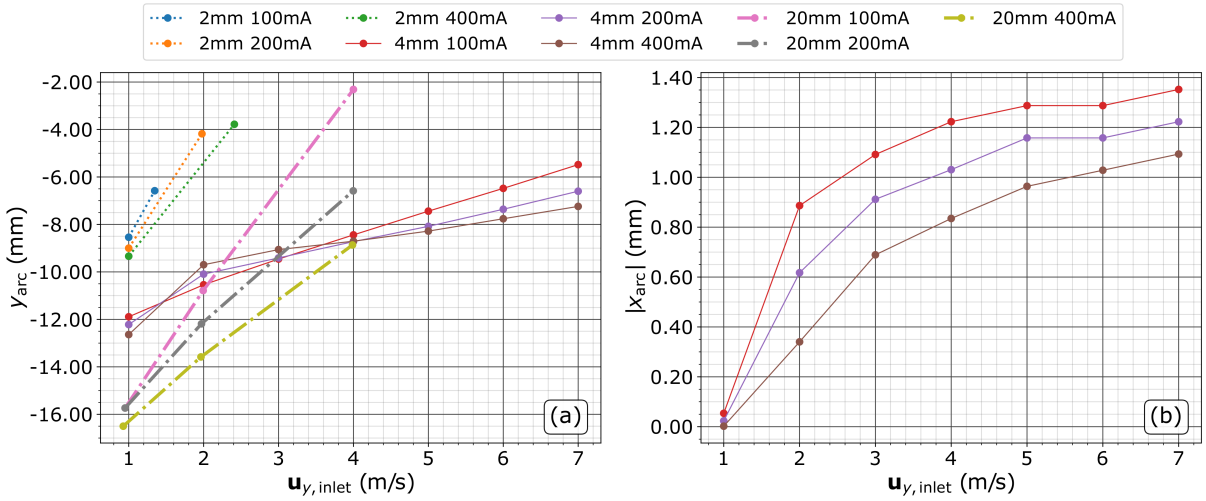

Figure 8: Position of the arc, related to the inlet gas flow velocity $\mathbf{u}_{y,\text{inlet}}$: **y**-position y_{arc} (a); absolute value of the **x**-position x_{arc} (b), (distance between the walls $x = 2$ mm).

The values for the position, in the $\mathbf{W_D} = 20$ mm cases, are obtained from averaging over one period of the transverse **x**-directed oscillations. At higher gas velocities, the arc is pushed downstream (up in the **y**-direction) due to the higher friction with the gas flow. The strongest friction with the gas is at the smallest distance between the walls $\mathbf{W}_\text{D} = 2$ mm. For the case of $\mathbf{W}_\text{D} = 4$ mm, the influence of the gas velocity on the position of the arc (y_{arc}) is weaker. This is probably related to the smaller ratio of the arc diameter to the inter-wall distance and the distance of the arc from the walls, both shown in figure 8(b).

It should be noted that the presented values for the simulations at $\mathbf{W}_\text{D} = 20$ mm, were found by averaging over several periods of the **x**-directed oscillations.

Summary of the results of the numerical study

The magnetic stabilization of the arc in the flow of gas represents an interesting configuration, from the point of view of fluid dynamics. The results show a strong influence of the channel walls on the arc stabilization. Three different types of behavior were observed in this study: 1) When the discharge operates between closely spaced side walls (separated by a distance less than twice the arc diameter), the arc stabilizes in the middle of the domain, mainly due to the presence of intense gas flow channels on both sides, that separate it from the walls; 2) When the distance between the walls is larger (several arc diameters), the arc tends to „attach“ to one of the side walls. This condition is energetically more favorable for the system, as it results in less friction between the gas and the arc, due to the lower gas velocity near the walls and the reduced gas pressure difference, due to the wider gas flow channel. 3) When the walls are at a large distance from the arc and the gas velocity is constant in the transverse direction, the arc becomes a source of vortices and instabilities occur in the gas flow. In this case, the well-known Karman vortex wake structure is observed. Since the arc is free to move, vortex-induced transverse oscillations of the arc occur.

In terms of arc stabilization, when the wall distance is small, the stabilization is much more difficult, because the gas drag is effectively higher and, for a given current, a stronger magnetic field needs to be applied. With a larger distance between the walls, the stabilization can be obtained more easily, because the arc is subject to less friction from the gas. In the case of a very large distance between the walls (or no walls), the arc begins to oscillate in the transverse direction, and the amplitude of this oscillation grows with the increase in the gas velocity. The transverse oscillations increase the friction of the arc with the gas, which reduces the ability of the magnetic force to stabilize the arc, at for a given vertical position.

With regard to gas treatment, the above-mentioned phenomena can interfere with the treatment effectiveness and reduce its efficiency at high gas velocities. Comparing the three cases identified, it can be concluded that in the second case, at the average distance between the walls, when the arc is localized to one of the side walls, the gas treatment might be higher. In the first case, with a small distance between the side walls, the arc stabilizes with difficulty, and in the case of a very large wall distance (channel width), a large part of the gas would remain untreated.

In laboratory tests, using a physical device, the effect of „sticking“ of the arc to one of the side walls, was indeed observed. This is presented in more detail, in chapter 3 of the dissertation document. The distance between the walls in the experiment is 2-4 times the diameter of the arc. This configuration corresponds to the simulated case with a wall spacing of $\mathbf{W}_{\mathrm{D}} = 4$ mm, considered in the numerical model.

Experimental measurements of CO_2 dissociation using different types of gliding arc discharges

In this part, as well as in chapter 3 of the dissertation, an experimental study of low-current DC discharges, with a gliding or stabilized arc, is presented. An experimental investigation of their applicability for dissociation of carbon dioxide was performed. The tests were done at the conditions of atmospheric pressure, for currents below 1 A. Publications related to this experimental study are [B.2, B.3]. Three types of discharges were studied, based on the classical configuration with flat, diverging electrodes. The first configuration is exactly the classical gliding arc setup, and the other two are variations of this concept, using external magnetic fields. In all configurations, the CO_2 gas is introduced from a nozzle, from the location of the smallest separation between the electrodes. Two quartz glasses located on the flat sides of the electrodes restrict the gas flow to the space between the electrodes and channel it through the plasma discharge. The choice to use the two-dimensional design with divergent electrodes is not accidental, since in this configuration the effect of applying a constant external magnetic field can be tested more easily.

In the second studied configuration, using an external magnetic field (created from permanent magnets), the arc speed is increased and the periods between ignition and extinction of the arc are shortened. The magnets are oriented in such a way, that the created external magnetic force „pushes“ the arc upwards (downstream), following the gas flow. In the third configuration, the arc is magnetically stabilized. In this case, the external magnetic force is oriented against the gas flow, and it slows down the arc. For

a given distance from the permanent magnets it becomes stationary. This configuration is studied using a computer model [B.1], and this study is presented in chapter 2 of the dissertation.

Since the discharges we studied, were found to operate both in the arc and glow regimes, it was decided to refer to them using the more general term „Gliding Discharge“ (GD), instead of „Gliding Arc“ (GA).

Mainly two quantities were measured. These are the conversion of CO_2 and the energy efficiency. Conversion is defined as the ratio of the dissociated gas, after plasma treatment, to the total quantity of gas that has entered the system. Energy efficiency is the ratio of the minimum amount of energy required to obtain the measured conversion, to the total energy consumed by the device. In general, the results show that the CO_2 conversion decreases at higher gas flow rates, and increases at higher values for the input power. Energy efficiency increases with increasing gas flow for all configurations. The magnetically stabilized configuration was found to have a more stable behavior and high efficiency for low gas flow rates, but at higher flow rates, it had a sharp drop in conversion. The nonstabilized configurations have high conversion values over a larger range of gas flows, but are unstable and less efficient than the magnetically stabilized discharge.

Experimental setup and discharge configurations

The experimental setup is presented schematically in figure 9. The gas discharge reactor, where the conversion takes place is marked in figure 9 as (2). The gas conversion reactor is a sealed, cylindrical glass tube, which remains at atmospheric pressure. The glass tube houses the discharge device, which consists of a pair of flat diverging electrodes, sandwiched between two quartz glasses, with permanent magnets placed on top of the glasses in the case of the magnetic configurations. Atmospheric pressure is maintained throughout the gas system. The input gas is introduced to the discharge device from a nozzle at its base. The inlet gas flow to the nozzle is controlled with mass flow controllers (MFC: Bronkhorst EL-FLOW F-201CM) – labeled in figure 9 as (1). Power is provided by a high voltage supply – figure 9(3), with a limited maximum current.

A single experimental measurement proceeds as follows. First, the flow rate of the inlet gas is set, using the mass flow controllers. The gas enters the glass tube of the dissociation device through the nozzle and passes through the plasma discharge. The glass tube has an outlet connected to the outside atmosphere, so some of the processed gas escapes through this outlet, maintaining the pressure inside the tube 1 atm.

After the system is filled with the converted gas, a sample of the gas mixture is withdrawn for analysis and the discharge is turned off. The sample is fed to a Fourier Infrared Spectrometer (FT-IR) – figure 9(6). The absorption spectrum of the gas sample is measured by the FT-IR. The measured absorption spectrum is relative to a background (reference) spectrum measurement, of a sample containing only CO_2. To find the conversion of the gas sample, the absorption value of a specific line (at wave number 2209 cm^{-1}) of the carbon monoxide CO molecular band is measured. The conversion measurements are calibrated by a separate series of absorbance measurements of samples containing a calibration mixture of CO_2 + CO, with guaranteed high accuracy of the ratio between

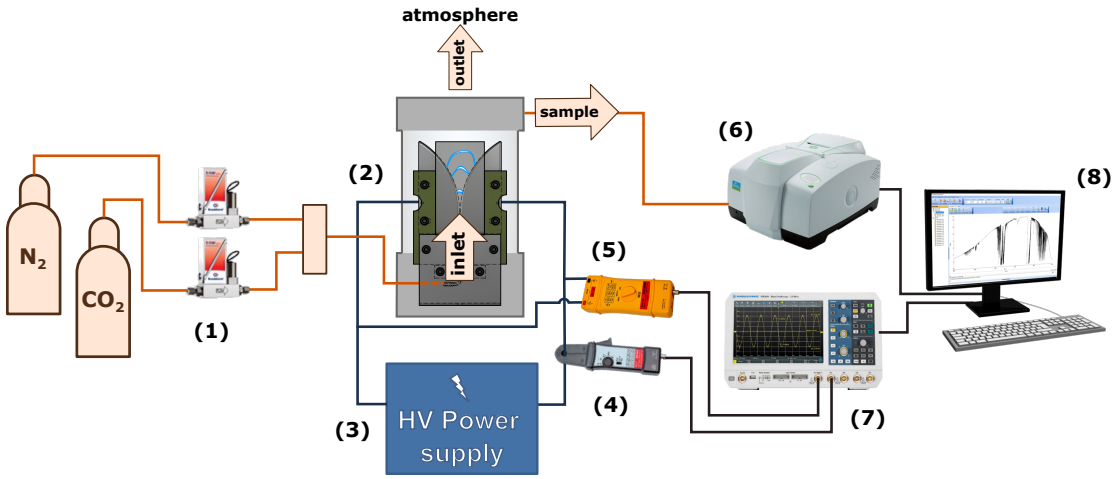

Figure 9: Schematic diagram of the experimental system components – mass flow controllers (1), conversion reactor (2), high voltage supply (3), current probe (4), high voltage probe (5), FT-IR spectrometer (6), oscilloscope (7), data processing computer (8).

the two gases.

Oscillograms of the voltage drop, between the discharge electrodes, and of the current through the discharge are recorded. These waveforms are used to calculate the average power input to the discharge. The voltage and current measurements are done using a high voltage differential probe (Pintek DP-30K) – figure 9(4) and a current probe (Pintek PA-699) – figure 9(5).

Discharge configurations

Three different discharge (GD) configurations were tested. These are the configuration of Non-Stabilized Gliding Discharge (NSGD), Magnetically-Stabilized Gliding Discharge (MSGD) and Magnetically-Accelerated Gliding Discharge (MAGD). These three types are represented schematically in figure 10. Figure 10(a) shows the dimensions of the separate parts of the discharge device. Similar devices are used in [12, 13, 15, 31].

Two types of materials were tested for the electrodes: aluminum and stainless steel (SS, ALSI 304). For all discharge configurations, the plasma is confined to the space between the electrodes, by a pair of quartz glasses. The metal electrodes are „pressed“ between these glasses. This ensures that a larger portion of the input gas interacts with the plasma. Additionally, these glasses are critical for magnetic configurations, because they isolate the magnets from the metal electrodes to ensure no short circuits occur.

The gas is supplied to the discharge device from its bottom side, where the distance between the electrodes is the smallest. The width of the nozzle, from where the gas is supplied, is 3 mm, which is equal to the distance between the glasses, also equal to the thickness of the electrodes.

For the magnet configurations – MSGD and MAGD, a pair of permanent NbFeB magnets are placed on top of the quartz glasses, that is, there is one magnet on the

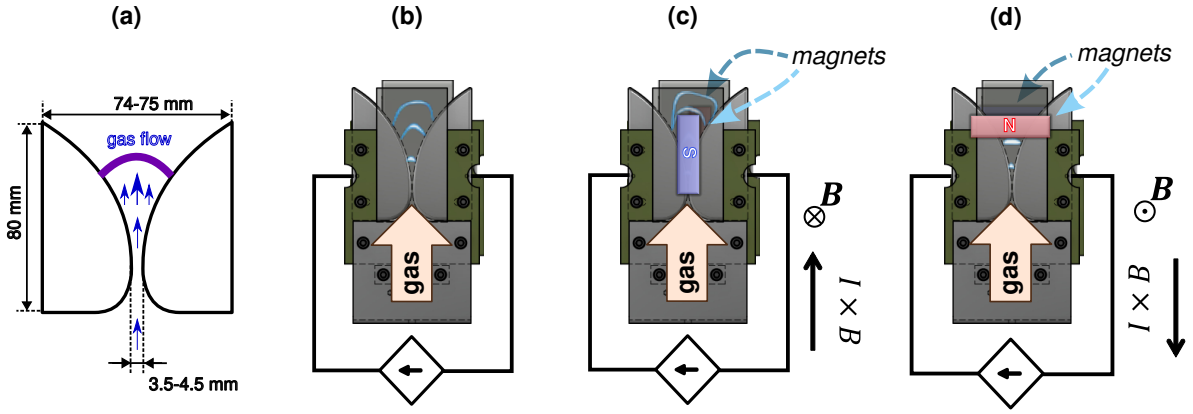

Figure 10: Dimensions of the discharge device parts (a) and schematics of the three types of discharge configurations – non-stabilized gliding discharge (NSGD) (b), magnetically accelerated gliding discharge (MAGD) (c) and magnetically stabilized gliding discharge (MSGD) (d).

outside of each of the two quartz glasses. The two magnets create a strong magnetic field of $\approx 0.5 - 0.6$ T in the space between the electrodes, and remain fixed on the glass faces, due to their mutual attraction. The orientation of the magnets, relative to the electrodes, determines the direction of the magnetic force experienced by the arc. For the magnetically accelerated MAGD configuration, the magnetic force is directed upward (in the direction of the gas flow), so the arc gliding velocity increases. In the magnetic stabilization MSGD configuration, the magnetic force is directed downward, or against the gas flow, and the arc stabilizes at the place, at which the gas resistance equalizes with the magnetic force.

For the MAGD setup, the magnets are oriented vertically, as illustrated in figure 10(c). This ensures that the arc experiences the action of the magnetic field for a longer period of time as it moves („glides“). For MSGD – figure 10(d), the magnets are in a horizontal orientation, located at a specific position above the inlet nozzle. This creates a magnetic „barrier“, that slows down and eventually stops the movement of the arc, creating the so-called magnetically stabilized arc.

NSGD configuration – Non-Stabilized Gliding Discharge The non-stabilized configuration (NSGD) – figure 10(b), uses the classic GD (GA) design, where the combined effect of arc drag with the gas flow and thermal advection acting on the hot gas in the arc, acts to push and extend the plasma arc along the electrodes – a gliding discharge.

MAGD configuration – Magnetically Accelerated Gliding Discharge In the MAGD configuration – figure 10(c), an external magnetic field creates an additional magnetic force in the direction of the gas flow. This increases the speed of the arc and shortens the period between ignition and extinction.

MSGD configuration – Magnetic Stabilized Gliding Discharge In the magnetically stabilized configuration (MSGD) – figure 10(d), the orientation of the magnetic field is such that the magnetic force experienced by the arc is in the opposite direction to the

drag force, from the gas flow. In this way, the magnetic field stabilizes the discharge at a certain position along the electrodes, where the two forces equalize. The stabilized arc remains stationary, with quasi-constant parameters in time. Obviously, this stabilization cannot take place for large gas flow rates. This configuration has also been investigated by the means of a computer model, described in chapter 2 of the dissertation document.

High voltage power supply

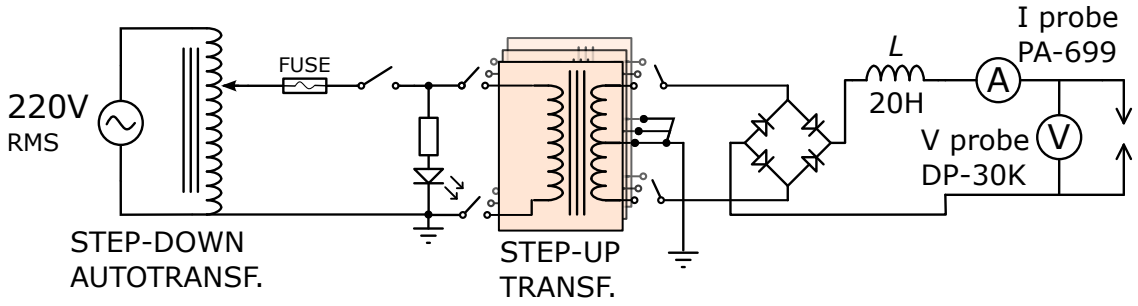

Figure 11: Electrical circuit diagram of the high voltage power supply, used in the experiments.

For the power supply used in these experiments, one of the goals was to minimize the ohmic losses. For the used power supply, the maximum current is not limited by a series resistor, but is instead limited by the step-up transformer itself. The electrical schematic of the power supply is presented in figure 11. Setting the maximum discharge current is done by mechanically switching between one of several step-up neon transformers – SIET Metalbox 10 kV (effective AC voltage). Each one of these transformers, has a different value of its maximum secondary winding current, from 25 mA to 110 mA. By connecting two of these transformers in parallel, currents of 210 mA can also be achieved. There is a large inductance connected in series with the discharge, which acts as a low-pass filter. This device succeeds in partially filtering the rectified voltage after the bridge rectifier (Graetz circuit).

With the current power circuit design, the supply voltages and currents are not filtered well enough, so there is still a significant AC component at 100 Hz. This can be seen in the current and voltage waveforms, shown in figure 12. Insufficient filtration can cause intermittent arcing, resulting from large voltage drops.

As an improvement, a new design for a three-phase power supply was considered. This supply though, was not used in the current experiments. In the future, the use of a more complex power supply, like a switch mode power supply, is also viewed as an option, as this kind of power circuits can achieve high energy efficiencies and also allow for smooth regulation in a wide interval of voltages and currents.

Measured quantities and their uncertainties

The most frequently measured quantities in other studies in the literature, including in [2, 14, 15, 31] are: 1) CO_2 conversion, 2) Specific Energy Input (SEI), and 3) the energy efficiency of the process. These are also the quantities that are measured in the current

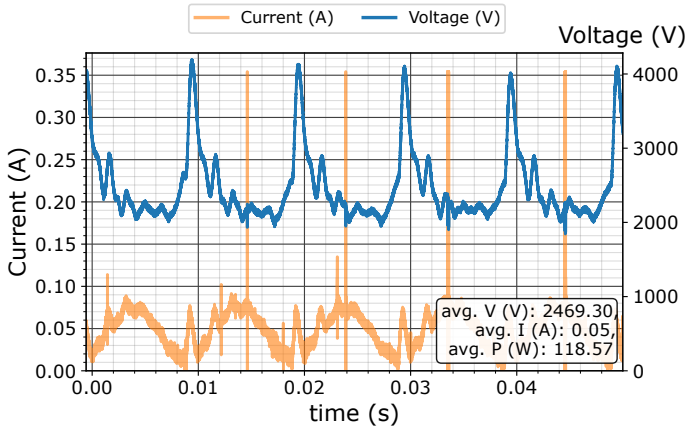

Figure 12: Representative oscillogram for the MSGD configuration. For the presented measurement, the maximum current in the secondary winding of the step-up transformer is 50 mA, and the input gas flow rate is 6 Ln/min.

experimental work.

The quantity **conversion** is defined as the fraction (or percentage) of the converted CO_2 gas:

$$X_{CO_2}, \% = \frac{N^{\text{init}}_{CO_2} - N^{\text{final}}_{CO_2}}{N^{\text{init}}_{CO_2}} \times 100\ \% = X_{CO_2} \times 100\ \%, \tag{12}$$

where $N^{\text{init}}_{CO_2}$ is the initial concentration of CO_2, and $N^{\text{final}}_{CO_2}$ is the final one, after the conversion process. For our experiments, the conversion of CO_2 was measured from the relative absorption spectrum of a sample of the treated gas. The absorbance is measured for a specific line in the spectrum of the CO molecule, at 2209 cm^{-1}, and is proportional to the concentration of carbon monoxide CO in the sample. The percentage of conversion can be directly obtained from it, and the two quantities are assumed to be linearly dependent. By introducing the proportionality factor α, this dependence can be expressed as $X^0_{CO_2} = \alpha I_{\text{absorb}}$, where $X^0_{CO_2}$ is in the interval $[0, 1]$. The value of the coefficient α was found with sufficiently high accuracy, by a separate series of measurements, in which a reference gas mixture of 20 % CO and 80 % CO_2 was used. In order for the measured conversion $X^0_{CO_2}$ to meet the definition given in the equation 12, it must be corrected to account for the expansion of the input carbon dioxide gas, upon its dissociation, as our setup remains at constant atmospheric pressure at all times. The corrected value is obtained, from the measured one, by the following relationship:

$$X_{CO_2} = \frac{2X^0_{CO_2}}{(3 - X^0_{CO_2})}. \tag{13}$$

The detailed derivation of equation 13 is done in chapter 3 of the dissertation document (in section 3.3.1).

Specific energy input – SEI [J/mol] is the average energy input for one mole of gas. This quantity can be expressed from the gas flow rate and the power P introduced into

the discharge, as:

$$\text{SEI [J/mol]} = \frac{P \text{ (J/s)}}{Q \text{ (Ln/s)} \times (1/22.4) \text{ (mol/Ln)}}, \tag{14}$$

where Q (Ln/s) is the value of the gas flow rate in Ln/s and P is the average power input to the discharge.

Energy efficiency η is defined as the ratio of the minimum energy required to convert X_{CO_2}, to the total energy consumed by the device. It can be expressed in terms of the specific energy input SEI as:

$$\eta = \frac{X_{CO_2} \times \Delta H_R}{\text{SEI}} \times 100 \text{ \%}, \tag{15}$$

where $\Delta H_R = 279.8 \times 10^3$ [J/mol] is the enthalpy of the CO_2 splitting reaction.

The expressions for the uncertainties, of the individual measured and calculated quantities, are presented in detail in chapter 3 of the dissertation (section 3.3.4). For the available experimental results, using these expressions, it is calculated that the relative uncertainty in the conversion X_{CO_2} is around $10 \text{ \%} - 12 \text{ \%}$ and the relative uncertainty for the energy efficiency η is about $15 - 17$ %, again noting that these percentages are relative to the absolute values of these quantities.

Results and discussion

Over 400 measurements were made, where the maximum discharge current (the maximum current through the secondary winding of the step-up transformer) was varied from 25 to 210 mA. The discharges were tested at different gas flows in the range from 1 to 14 Ln/min. Additional measurements were made, using a modification of the non-stabilized NSGD configuration, without quartz side glasses. This configuration is labeled in the results as NQNSGD (No quartz non-stabilized gliding discharge).

Results for the conversion and the energy efficiency

Figure 13 presents the measured values for the conversion and energy efficiency for all performed experiments, against the power and the specific energy input SEI. Regardless of the type of discharge, for values of SEI > 4 kJ/Ln, the conversion seems not to change significantly and remains semi-constant. The opposite is true for the energy efficiency, which decreases with increasing SEI, which is quite natural, since energy efficiency is inversely proportional to SEI (see equation 15). The maximum values for the conversion are around 8 %, while for the energy efficiency there are measured values above 40 %, which is a relatively good result. The optimal interval for SEI, where the efficiency and the conversion both have high values, seems to be between $2-4$ kJ/Ln, and in this interval the conversion is about $5 - 6$ % and energy efficiency is around $18 - 30$ %.

From figure 14, presenting the comparison between the three different types of discharges, it can be seen that for a flow rate above 3 Ln/min, the highest measured conversion values are for the NSGD configuration, while below 3 Ln/min, the best results for both conversion and energy efficiency are obtained with the magnetically stabilized

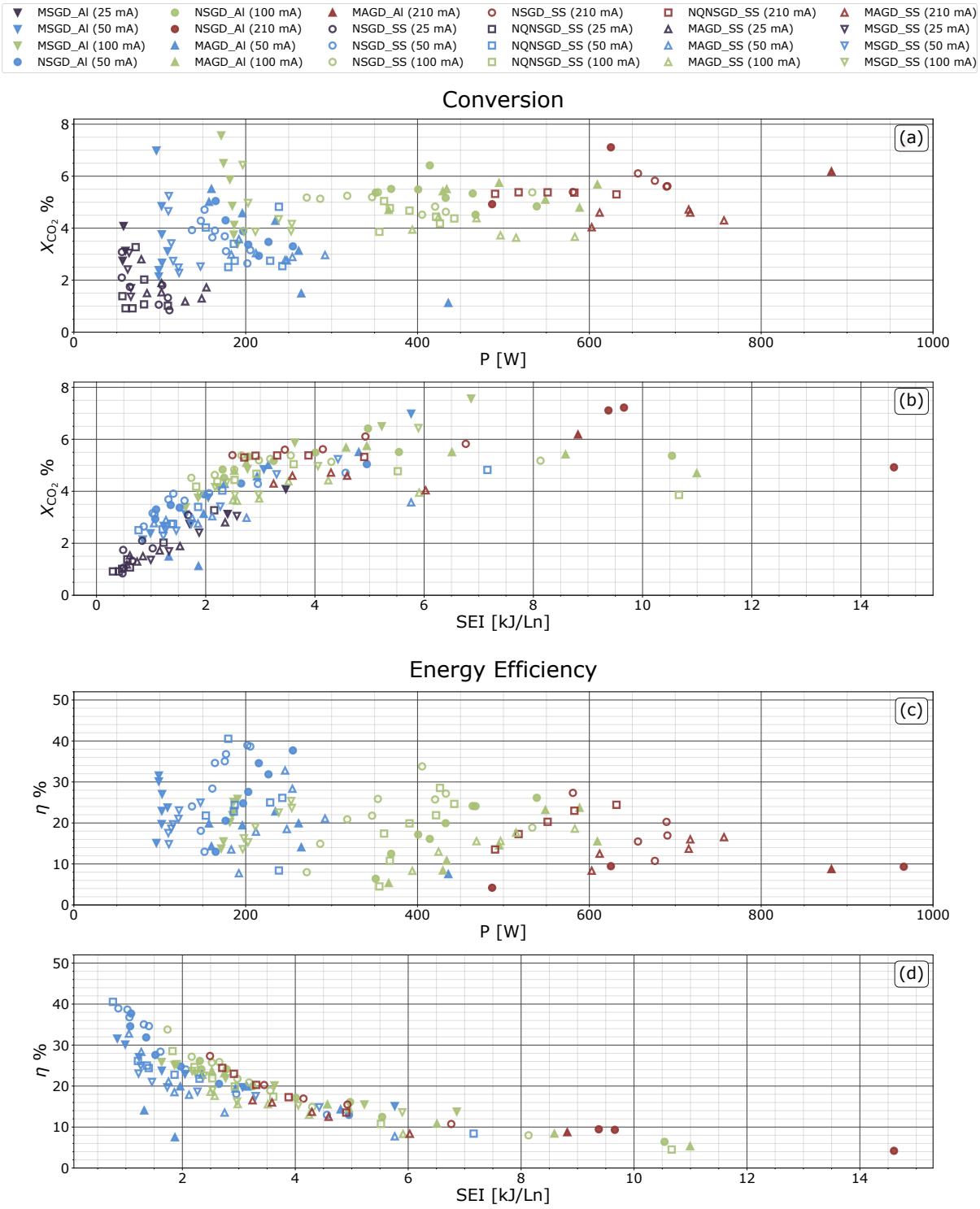

Figure 13: Measured conversion (a, b) and energy efficiency (c, d), for the three different configurations, for the two different electrode materials (SS – stainless steel, Al – aluminum), at different currents (as indicated in legend). The results are given against the input power P (a, c) and SEI (b, d). Markers: ▼ MSGD, ● NSGD, ▲ MAGD, ■ NQNSGD, filled marker - aluminum electrodes, empty marker - stainless steel electrodes. The color indicates the maximum value of the discharge current, which is an input parameter that depends on the choice of the connected transformer.

MSGD configuration. The discharge in the magnetically accelerated MAGD configuration, when compared to the classical NSGD variant, has lower values for both conversion and energy efficiency, under these conditions. This may be attributed to the fact, that in the MAGD configuration, the arc extends more and therefore dissipates more power due to the larger average voltage drops.

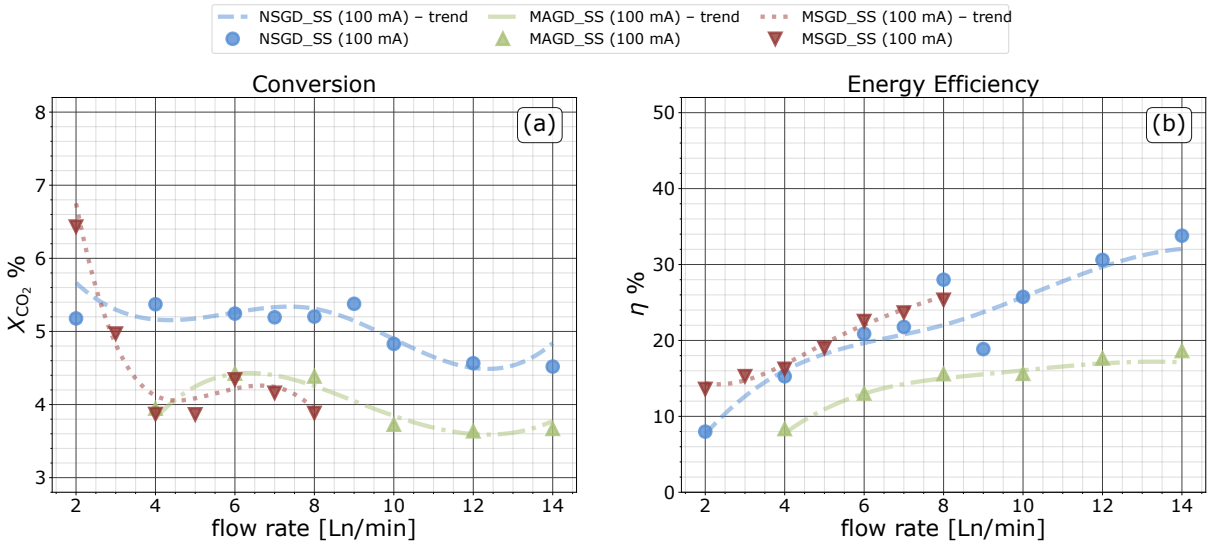

Figure 14: Comparison of the conversion (a) and energy efficiency (b), between the three different types of discharges, at a maximum discharge current of 100 mA, for the stainless steel electrodes.

Additional tests were made on the non-stabilized version of the discharge with the side quartz glasses removed. These measurements are labeled as the NQNSGD series. From the comparison made, shown in figure 15, it can be seen that for all tested flow rates, there is a constant relative difference for both the conversion and the energy efficiency. At 2 Ln/min, this difference is the largest – about 25 %. This effect can be explained by the fact that, for the same gas flow rate, the configuration with the glasses removed has a larger effective area for the gas to flow, and therefore the gas will have a lower average velocity. For the same operating time, in the variant without glasses, the processed gas would be less, as it is observed. From this comparison, it can be concluded that the presence of limiting side glasses has a positive effect.

Figure 16 compares measurements made with aluminium and steel electrodes, at 100 mA, for the non-stabilized NSGD configuration. The results for aluminium (Al) electrodes show relatively higher values for conversion but lower for energy efficiency. In absolute terms, the conversion is up to 1 % higher for the case of aluminum electrodes, but only at moderate flow rate ($4 - 10$ Ln/min). Stainless steel electrodes are better in terms of energy efficiency, having up to 10 % higher efficiency values, at higher flow rates. The substantial difference in the conversion can be partly explained by the fact that aluminium has a higher thermal conductivity – for the alloy used (Al) $k_{Al} \approx 190$ $\mathrm{Wm^{-1}K^{-1}}$, and for the SS material it is $k_{SS} \approx 14.4$ $\mathrm{Wm^{-1}K^{-1}}$ (stainless steel, type 304).

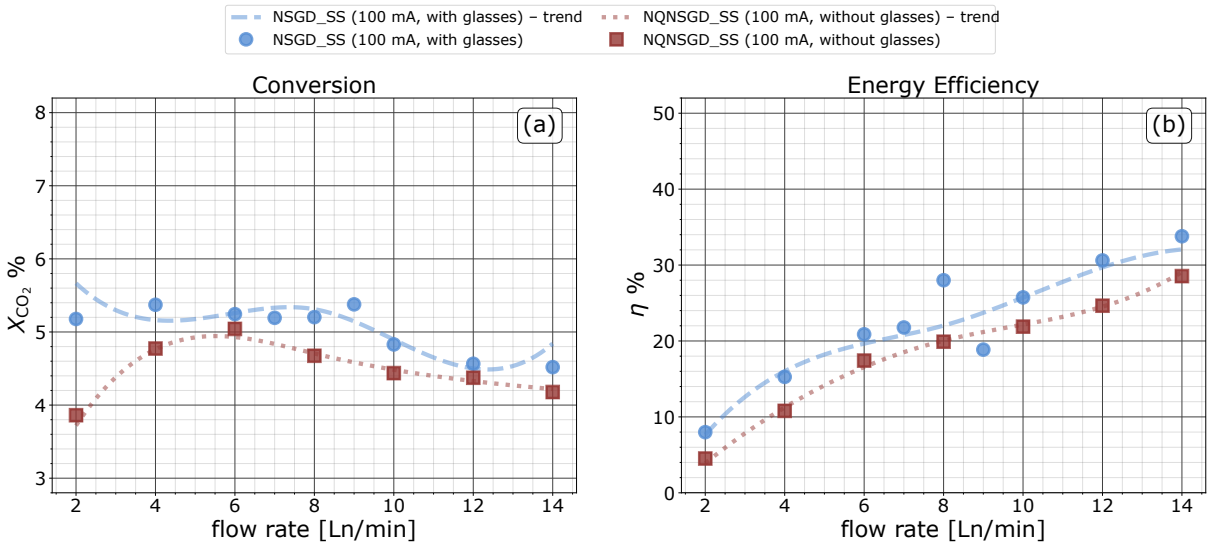

Figure 15: Comparison of the conversion (a) and energy efficiency (b), for the NSGD discharge variant, with and without side quartz glasses, at a maximum current of 100 mA.

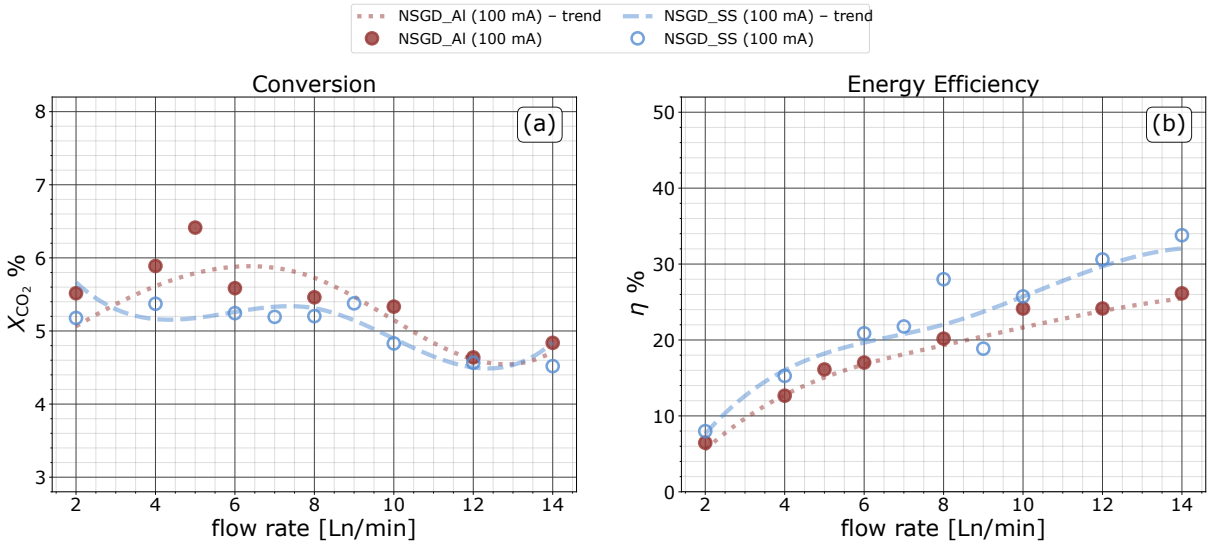

Figure 16: Comparison of the conversion (a) and energy efficiency (b) measurements, for the two different types of electrode materials used. Measurements are shown for the NSGD configuration, at a maximum current of 100 mA.

Qualitative explanation of the plasma discharge behavior

In the non-stabilized and magnetically accelerated configurations (NSGD and MAGD), when the arc forms, it is initially bright and small in diameter. At this time, the arc has high core temperature in the positive column, and is strongly contracted. Figure 17(a) shows a photograph of the evolution of the arc over time, taken with a fast camera, with an exposure time of 1 μs and intervals of 2 ms between successive photos.

At a later stage, after the initiation, the arc has a wider positive column, with a weaker glow, indicating a lower gas temperature and a state of temperature non-equilibrium

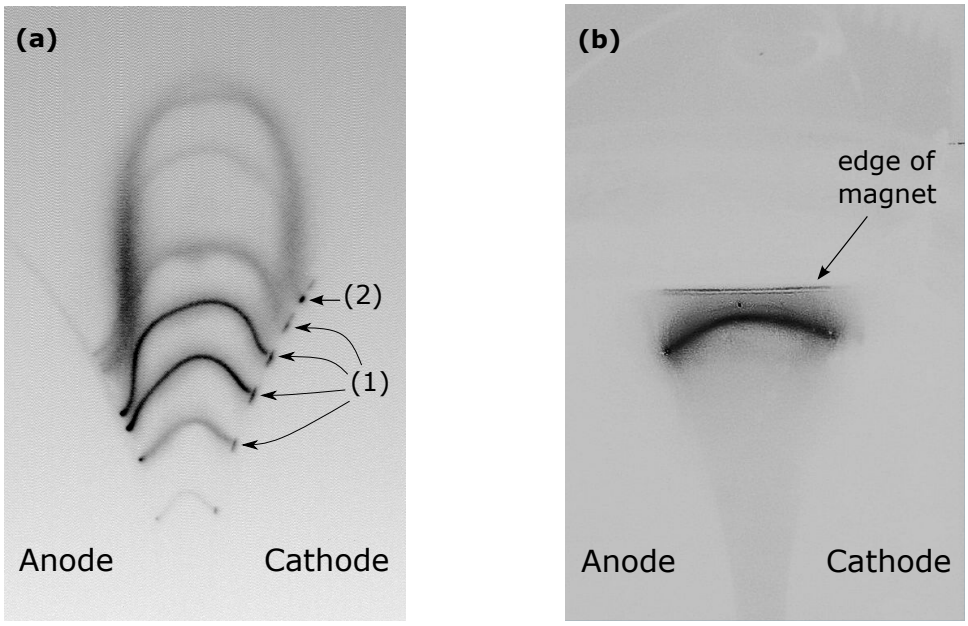

Figure 17: In subfigure (a): Combined picture (negative) of the evolution of the arc over time, taken with a fast I-CCD camera PI-Max with a combined 10 exposures, of length 1 μs each, separated by intervals of length 2 ms. The current through the discharge has a maximum value of 100 mA, the flow rate is 4 Ln/min, using the NSGD type of discharge. Points (1) are the negative glow cathode regions of the discharge, for the case of glow discharge operating mode. Point (2) is probably a cathode spot and is a sign of a transition to an arc mode of discharge. In subfigure (b): Photograph (negative) of a stationary, stabilized arc in the magnetically-stabilized MSGD configuration, taken with an exposure time on the order of ms. The current through the discharge is limited to 50 mA, the gas flow rate is 5 Ln/min, in the magnetically stabilized configuration MSGD.

between the electrons and the heavy particles in the plasma. As the arc „glides“ along the electrodes, the discharge appears to have a broad cathode region and a brighter glow in the near-cathode region. This is typical of a glow discharge supported by secondary electron emission, and the bright spot in the cathode space is from the negative glow region [34]. At low current values, on the order of hundreds of mA and lower, it was found that the discharge can operate in both arc and glow modes [35, 36, 37, 38], depending on cathode surface conditions, working gas, and plasma dynamics. Similar behavior, of low-current discharges at atmospheric pressure, was also observed in [35, 37].

Regarding the application of the discharge for CO_2 dissociation, the mode of the cathode region (glow/arc) probably plays an important role. Assuming that the additional power in the glow mode does not contribute to gas processing (gas processing occurs primarily in the positive column), then the glow mode would be expected to have $5-10$ % lower efficiency compared to the arc one.

For the NSGD configuration, the field was roughly found to be about $2000-2600$ Vcm^{-1} for a discharge length of $10-15$ mm, about $1000-1500$ Vcm^{-1} for lengths of $15-40$ mm and below 1000 Vcm^{-1} for lengths of $40-80$ mm. For the magnetically stabilized configuration the electric field in the positive column was found to be in the approximate range

$1200 - 1800$ Vcm^{-1} , which is of the same order as for non-stabilized discharges of similar length.

Using photographs of the MSGD configuration in operation, the diameter of the (visible) light-emitting part of the arc was measured to be between $1 - 2$ mm, which depends strongly on the current. Since that, at the studied currents ($\sim$ 100 mA), the effective diameter of the arc is smaller than the distance between the quartz glasses (equal to the width of the electrodes of 3 mm), the arc is pushed close to one of the side walls. This behavior was predicted in [B.1], and is also described in more detail in chapter 2 of the thesis.

Summary of the experimental research results

Through the conducted experiments, the properties of three types of gliding arc discharges were investigated and their applicability for the dissociation of CO_2 was evaluated. A comparison was made between the three types of discharges, through the main quantities - the conversion (the ratio of the converted gas to the absorbed gas) and the energy efficiency of the process.

The simplest configuration of the non-stabilized discharge NSGD, showed good results in a wide range of gas flow rates. The magnetically accelerated MAGD configuration surprisingly performed less well than the non-stabilized NSGD, but overall both configurations had similar performance. The magnetically stabilized variant MSGD shows good conversion and energy efficiency at low values of the gas flow rate, but these decrease rapidly with increasing flow, and for flow rates above $7 - 9$ Ln/min, the arc can no longer be magnetically stabilized.

The addition of quartz side glasses to the discharge device was found to have a positive effect on both the conversion and the energy efficiency. It was also found, that the performance of the device depends on the type of electrode material. Aluminium electrodes showed better values for conversion than the stainless steel electrodes, with a relative difference of about 10 %, but the stainless electrodes had higher values for the energy efficiency. One possible explanation for this is that, in the case of aluminum electrodes, the gas temperature in the region near the plasma can be kept relatively lower, due to the higher thermal conductivity of aluminium compared to the stainless steel alloy. This could explain the higher conversion values in the case of aluminium electrodes.

Despite the differences in the three discharge configurations, the results for the CO_2 conversion and energy efficiency follow similar general trends from SEI, indicating the importance of this parameter.

Our research has shown that under the conditions of low current discharges, up to 210 mA in our case, in the non-stabilized configurations (NSGD and MAGD), the discharge can be maintained in both glow and arc modes. The device has a reduced efficiency, when operating in glow mode, due to the significant voltage drop in the cathode region. In this case, there are additional power losses associated with the heating of the gas near the cathode and the heating of the cathode surface itself. It can be concluded that the discharge would work more optimally, if it could be limited to operate in the arc mode.

The two-dimensional diverging electrode geometry allows the testing of various types of modifications of the classic gliding arc discharge, including those with magnetic stabilization in cross-gas flow. In this work, a configuration with magnetic stabilization was tested and successfully compared to the classical gliding discharge configuration, with and without quartz side walls. A magnetically accelerated arc configuration was also tested. The magnetically stabilized configuration showed good performance, both for the conversion and the energy efficiency, but only at low gas flow rates.

Conclusion

In the course of this doctorate, both theoretical and experimental studies were done, of low-current gliding discharges, with and without magnetic stabilization, to which there are several publications – [B.1, B.2, B.3]. The first study is related to a numerical model of a low-current arc discharge, with applied magnetic stabilization, at atmospheric pressure. Other similar studies have been done mainly for arc discharges at higher currents and are based on experimental studies [39, 40, 22, 41, 42]. For this reason, it can be said that the results of the performed simulations with our model can be useful for understanding the processes at lower currents $\sim 10^{-1}$ A.

The second part of the doctoral work is the experimental investigation of the properties of several types of low-current arc discharges for CO_2 dissociation, including those with magnetic stabilization. Mainly two quantities are studied – the conversion and the energy efficiency. The measured values for the conversion under some conditions reach up to 7-8% and for the energy efficiency values above 30% are recorded, and these results compare well with the ones from other similar studies [12, 13, 15, 31].

A Main results and contributions of the dissertation

The main contributions of the dissertation can be summarized as follows:

- A two-dimensional fluid model of a cross-section of the positive column of an arc (or glow) discharge, has been developed, at conditions of non-equilibrium plasma, at atmospheric pressure, with consideration of the effect of an external magnetic field.
- Using the developed fluid model, the approximate ranges of gas velocities (at various conditions), at which magnetic arc stabilization can be achieved, have been found.
- From the results obtained with the model, different stable and unstable regimes of low-current magnetically stabilized arcs have been identified, in a gas flow transverse to the current of the arc: a) Arc stabilized in the middle of the gas channel, as a result of cooling from side walls; b) Unstable arc that deviates to regions of low gas velocity and stabilizes near the walls; c) Unstable and oscillating arc (flutter instability [33]), with widely spaced side walls and homogeneous gas flow.
- Some of the main characteristics of a magnetically stabilized arc in a gas flow have been obtained, and its behavior has been investigated, applying a model of a solid body in a moving fluid. Values for the drag force and the effective drag coefficient of

the arc, with the gas flow, were calculated. An estimate was made, for the effective radius of the positive column of the arc.

- Various configurations of gliding and stabilized arc (glow) discharges were experimentally investigated, and their applicability for carbon dioxide dissociation was evaluated.
- The effect of a transverse instability, for a magnetically stabilized arc in a gas flow, for a flow channel wider than its effective radius, which was predicted by numerical model simulations, was experimentally confirmed.
- A qualitative analysis of the discharge mode in relation to cathodic processes was made, for currents ≤ 100 mA, at atmospheric pressure, in carbon dioxide, thus it was established that the discharge can work both in glow mode, as well as in arc mode.
- Using experimentally measured values for electrical parameters, together with photographs taken with a high-speed camera, approximate values for the current density and electric field intensity, in the region of the positive column of the arc, were found, for the studied discharges in CO_2.

Personal contributions

- Participated in the design and fabrication of the experimental setup, including the discharge reactor, high voltage power supply and additional peripherals to the setup.
- Software was developed for processing the experimental results of the measurements.

B List of publications included in the dissertation

Articles in scientific journals with an impact factor:

1. V Ivanov, Ts Paunska, Kh Tarnev and St Kolev **2021** Magnetic field stabilization of low current DC arc discharge in cross flow in argon gas at atmospheric pressure – a numerical modelling study *Plasma Sources Sci. Technol.* **30** 085007 **Quartile: Q1, Impact factor: 4.004 (Scopus)**
2. V Ivanov, Ts Paunska, S Lazarova, A Bogaerts and St Kolev **2023** Gliding arc/glow discharge for CO_2 conversion: Comparing the performance of different discharge configurations *J. CO2 Util.* **67** 102300 **Quartile: Q1, Impact factor: 7.84 (Scopus)**

Scientific conference papers published in full text:

3. V Ivanov, S Lazarova, S Iordanova, Ts Paunska, N Georgiev and St Kolev **2022** Conversion of CO_2 in stabilized low-current arc discharge at atmospheric pressure *J. Phys.: Conf. Ser.* **2240** 012029, **Quartile: Q4**

C Participation in scientific conferences

- 2022, *48th European Plasma Physics conference*, poster on „Gliding arc discharge for CO_2 conversion: An experimental study of different discharge configurations“, V Ivanov, Ts Paunska, S Lazarova, S Iordanova and St Kolev
- 2021, *VEIT conference*, presentation on the topic „Magnetic field stabilization of DC arc in cross gas flow“, V Ivanov, Ts Paunska, Kh Tarnev and St Kolev
- 2021, *47th European Plasma Physics conference*, poster on „Magnetically stabilized gliding arc discharge: A 2D model “, V Ivanov, Ts Paunska, S Lazarova, S Iordanova and St Kolev. Won first prize for best poster in the category of Low Temperature and Dusty Plasmas (LTDP)

Bibliography

[1] Home – climate change: Vital signs of the planet (https://climate.nasa.gov/), 2022.

[2] Ramses Snoeckx and Annemie Bogaerts. Plasma technology – a novel solution for CO2 conversion? *Chem. Soc. Rev.*, 46:5805–5863, 2017.

[3] Robby Aerts, Wesley Somers, and Annemie Bogaerts. Carbon Dioxide Splitting in a Dielectric Barrier Discharge Plasma: A Combined Experimental and Computational Study. *ChemSusChem*, 8(4):702–716, 2015.

[4] R. Snoeckx, S. Heijkers, K. Van Wesenbeeck, et al. CO2 conversion in a dielectric barrier discharge plasma: N2 in the mix as a helping hand or problematic impurity? *Energy Environ. Sci.*, 9(3):999–1011, 2016.

[5] Danhua Mei and Xin Tu. Conversion of CO2 in a cylindrical dielectric barrier discharge reactor: Effects of plasma processing parameters and reactor design. *J. CO2 Util.*, 19:68–78, 2017.

[6] Marleen Ramakers, Inne Michielsen, Robby Aerts, Vera Meynen, and Annemie Bogaerts. Effect of Argon or Helium on the CO2 Conversion in a Dielectric Barrier Discharge. *Plasma Processes Polym.*, 12(8):755–763, 2015.

[7] G J van Rooij, D C M van den Bekerom, N den Harder, et al. Taming microwave plasma to beat thermodynamics in CO2 dissociation. *Faraday Discuss.*, 183:233–248, 2015.

[8] Mette Mikkelsen, Mikkel Jorgensen, and Frederik C Krebs. The teraton challenge. A review of fixation and transformation of carbon dioxide. *Energy Environ. Sci.*, 3:43–81, 2010.

[9] Constandinos M. Mitsingas, Rajavasanth Rajasegar, Stephen Hammack, et al. High Energy Efficiency Plasma Conversion of CO2 at Atmospheric Pressure Using a Direct-Coupled Microwave Plasma System. *IEEE Trans. Plasma Sci.*, 44(4):651–656, 2016.

[10] Masaharu Tsuji, Takeshi Tanoue, Kousuke Nakano, and Yukio Nishimura. Decomposition of CO2 into CO and O in a Microwave-Excited Discharge Flow of CO2/He or CO2/Ar Mixtures. *Chem. Lett.*, 30(1):22–23, 2001.

[11] Annemie Bogaerts and Gabriele Centi. Plasma Technology for CO2 Conversion: A Personal Perspective on Prospects and Gaps. *Front. Energy Res.*, 8, 2020.

[12] Antonius Indarto, Dae Ryook Yang, Jae-Wook Choi, et al. Gliding arc plasma processing of CO2 conversion. *J. Hazard. Mater.*, 146(1):309–315, 2007.

[13] Weizong Wang, Danhua Mei, Xin Tu, and Annemie Bogaerts. Gliding arc plasma for CO2 conversion: Better insights by a combined experimental and modelling approach. *Chem. Eng. J.*, 330:11–25, 2017.

[14] Li Li, Hao Zhang, Xiaodong Li, Jingying Huang, et al. Magnetically enhanced gliding arc discharge for CO2 activation. *J. CO2 Util.*, 35:28–37, 2020.

[15] Hao Zhang, Li Li, Xiaodong Li, Weizong Wang, et al. Warm plasma activation of CO2 in a rotating gliding arc discharge reactor. *J. CO2 Util.*, 27:472–479, 2018.

[16] Marleen Ramakers, Georgi Trenchev, Stijn Heijkers, Weizong Wang, et al. Gliding Arc Plasmatron: Providing an Alternative Method for Carbon Dioxide Conversion. *ChemSusChem*, 10(12):2642–2652, 2017.

[17] Antonin Berthelot and Annemie Bogaerts. Modeling of plasma-based CO2 conversion: lumping of the vibrational levels. *Plasma Sources Sci. and Technol.*, 25(4):045022, 2016.

[18] Tomas Kozak and Annemie Bogaerts. Evaluation of the energy efficiency of CO2 conversion in microwave discharges using a reaction kinetics model. *Plasma Sources Sci. Technol.*, 24(1):015024, 2014.

[19] A Fridman. *Plasma Chemistry*. Cambridge University Press, 2008.

[20] E K Scott. The manifacture of nitrates from the atmosphere. *Journal of the Royal Society of Arts*, 60, 1912.

[21] N Balcon, N Benard, P Braud, A Mizuno, G Touchard, and E Moreau. Prospects of airflow control by a gliding arc in a static magnetic field. *J. Phys. D: Appl. Phys.*, 41:205204, 09 2008.

[22] T W Myers and W C Roman. Survey of investigations of electric arc interactions with magnetic and aerodynamic fields, 1966.

[23] N Desaulniers-Soucy and J-L Meunier. Study of magnetically rotating arc stability using fluctuations in voltage, velocity and emission line intensity. *J. Phys. D: Appl. Phys.*, 28:2505–2513, 12 1995.

[24] S P Gangoli, A F Gutsol, and A A Fridman. A non-equilibrium plasma source: Magnetically stabilized gliding arc discharge: I. Design and diagnostics. *Plasma Sources Sci. Technol.*, 19:065003, 10 2010.

[25] S P Gangoli, A F Gutsol, and A A Fridman. A non-equilibrium plasma source: Magnetically stabilized gliding arc discharge: II. Electrical characterization. *Plasma Sources Sci. Technol.*, 19:065004, 10 2010.

[26] H Zhang, C Du, A Wu, Z Bo, J Yan, and X Li. Rotating gliding arc assisted methane decomposition in nitrogen for hydrogen production. *Int. J. Hydrogen Energy*, 39:12620–12635, 08 2014.

[27] H Zhang, G Trenchev, X Li, Y Wu, and A Bogaerts. Multi-dimensional modelling of a magnetically stabilized gliding arc plasma in argon and CO2. *Plasma Sources Sci. Technol.*, 29(4):045019, 2020.

[28] Z Feng, N Saeki, T Kuroki, M Tahara, and M Okubo. Magnetic-field-assisted gliding arc discharge plasma for surface modification. *IEEE Trans. Plasma Sci.*, 39:2846–2847, 11 2011.

[29] Fridman, A. *Plasma Chemistry*. Cambridge University Press, 2008.

[30] Jing-Lin Liu, Hyun-Woo Park, Woo-Jae Chung, and Dong-Wha Park. High-Efficient Conversion of CO2 in AC-Pulsed Tornado Gliding Arc Plasma. *Plasma Chem. Plasma Process.*, 36(2):437–449, 2015.

[31] Seong Cheon Kim, Mun Sup Lim, and Young Nam Chun. Reduction Characteristics of Carbon Dioxide Using a Plasmatron. *Plasma Chem. Plasma Process.*, 34:125–143, 2013.

[32] T Nunnally, K Gutsol, A Rabinovich, A Fridman, A Gutsol, and A Kemoun. Dissociation of CO2 in a low current gliding arc plasmatron. *J. Phys. D: Appl. Phys.*, 44(27):274009, 2011.

[33] R D Blevins. *Flow induced vibration*. Krieger Publishing company, 2001.

[34] Y Raizer. *Gas Discharge Physics*. Springer-Verlag, 1991.

[35] Y D Korolev, O B Frants, N V Landl, V G Geyman, and A I Suslov. Parameters of a positive column in a gliding glow discharge in air. *Phys. Plasma*, 24(10):103526, 2017.

[36] Y D Korolev, O B Frants, V G Geyman, et al. Low-Current "Gliding Arc" in an Air Flow. *IEEE Trans. Plasma Sci.*, 39(12):3319–3325, 2011.

[37] Y D Korolev, O B Frants, N V Landl, A V Bolotov, and V O Nekhoroshev. Features of a near-cathode region in a gliding arc discharge in air flow. *Plasma Sources Sci. Technol.*, 23(5):054016, 2014.

[38] St Kolev and A Bogaerts. Similarities and differences between gliding glow and gliding arc discharges. *Plasma Sources Sci. Technol.*, 24(6):065023, 2015.

[39] J F Klein and Y Y Winograd. Electric arc stabilization in crossed convective and magnetic fields. *AIAA J.*, 7:1699–1703, 10 1969.

[40] M D Cowley. A boundary layer model for balanced arcs. Technical report, Fluid Mechanics Lab., Massachusetts Institute of Technology, 1967.

[41] C J Buczek, R J Freiberg, P P Chenausky, and R J Wayne. Magnetic stabilization of the plasma column in flowing molecular lasers. *Proc. IEEE*, 59:659–667, 04 1971.

[42] A M Essiptchouk, L I Sharakhovsky, and A Marotta. A new formula for the rotational velocity of magnetically driven arcs. *J. Phys. D: Appl. Phys.*, 33:2591–2597, 10 2000.